 doi:10.20944/preprints202001.0183.v1

Article

Sensitivity of radiative fluxes to aerosols in the ALADIN-HIRLAM numerical weather prediction system

Laura Rontu [1,*], Emily Gleeson [2], Daniel Martin Perez [3], Kristian Pagh Nielsen [4] and Velle Toll [5]

1 Finnish Meteorological Institute; laura.rontu@fmi.fi
2 Met Éireann, Ireland; emily.gleeson@met.ie
3 Agencia Estatal de Meteorologia, Spain; dmartinp@aemet.es
4 Danish Meteorological Institute; kpn@dmi.dk
5 Institute of Physics, University of Tartu, Estonia; velle.toll@ut.ee
* Correspondence: laura.rontu@fmi.fi

Abstract: The direct radiative effect of aerosols is taken into account in many limited area numerical weather prediction models using wavelength-dependent aerosol optical depths of a range of aerosol species. We study the impact of aerosol distribution and optical properties on radiative transfer, based on climatological and more realistic near real-time aerosol data. Sensitivity tests were carried out using the single column version of the ALADIN-HIRLAM numerical weather prediction system, set up to use the HLRADIA broadband radiation scheme. The tests were restricted to clear-sky cases to avoid the complication of cloud-radiation-aerosol interactions. The largest differences in radiative fluxes and heating rates were found to be due to different aerosol loads. When the loads are large, the radiative fluxes and heating rates are sensitive to the aerosol inherent optical properties and vertical distribution of the aerosol species. In such cases, regional weather models should use external real-time aerosol data for radiation parametrizations. Impacts of aerosols on shortwave radiation dominate longwave impacts. Sensitivity experiments indicated the important effects of highly absorbing black carbon aerosols and strongly scattering desert dust.

Keywords: aerosols, CAMS, NWP, ALADIN-HIRLAM, MUSC, direct radiative effect

1. Introduction

Aerosols are tiny solid and liquid particles suspended in the air. They cause direct radiative forcing through scattering and absorbing shortwave (SW) and longwave (LW) radiation in the atmosphere. They also alter cloud formation and precipitation efficiency by increasing droplet and ice particle concentrations. In this way aerosols also cause indirect radiative forcing.

Aerosols off-set a poorly quantified fraction of the greenhouse gas warming effect on the Earth's climate. In fact, the quantification of aerosol radiative forcing is more complex than that for greenhouse gases because aerosol mass and particle concentrations are highly variable in space and time. This is mainly due to the shorter atmospheric lifetime of aerosols. Spatial and temporal information on the physical and radiative properties of aerosols is required such as size distributions, dependence on relative humidity, refractive index and solubility of the particles.

Over recent decades substantial progress has been made in reducing uncertainties related to radiative forcing due to aerosols. This progress is due to advances in global modelling, theoretical developments and improved observations. Integrated weather-chemistry models [1–3] simulate the life-cycle of aerosols

 doi:10.20944/preprints202001.0183.v1

from their formation to their deposition and their dispersion in the atmosphere at time-scales of the order of several days. In such models the physicochemical processes evolve in an environment controlled by atmospheric large-scale dynamics. Advanced data assimilation, using reliable data about emission sources and conventional and space-born observations, is used to constrain the modelled processes. The Copernicus Atmosphere Monitoring Service's (CAMS) global reanalysis of atmospheric composition [4] has resulted in an extensive historical aerosol dataset. They also provide a continuous service that produces global forecasts of aerosols and chemical constituents in near real-time [5].

Bozzo et al. [6] describe the updated global aerosol climatology used in the European Centre for Medium-Range Weather Forecast (ECMWF) model. The authors show that the use of a 3D global aerosol climatology based on CAMS interim reanalysis [4] combined with updated aerosol inherent optical properties (IOPs) leads to a systematic improvement in lower troposphere temperature and wind forecasts over certain regions of the globe. Recent studies, such as those by [7,8], provide the motivation to improve how aerosols are taken into account in short-range regional numerical weather prediction (NWP) models and not just in global medium-range forecasting models and climate models [9–11]. During wildfires, desert dust intrusions, volcanic eruptions and enhanced anthropogenic emissions aerosol concentrations in the atmosphere may significantly exceed climatological values, which can influence the weather on local to global scales. In such cases reliance on aerosol climatologies is insufficient for accurate forecasting of radiation and temperatures [12–14].

The direct radiative effect of aerosols on weather and climate is much better quantified than indirect effects [15,16] because of the better physical understanding of the aerosol radiative effects compared to the impact of aerosols on clouds and precipitation. This suggests in the limited area NWP models to focus on further improvement of aerosol radiative transfer parametrizations. The availability of up-to-date global aerosol datasets opens new possibilities for limited area NWP. It becomes less necessary to build regional integrated weather-chemistry models [17] when the weather models can import ready-made aerosol concentrations for use in parametrizations of radiative transfer, cloud-precipitation microphysics, and the consistent treatment of cloud-aerosol-radiation interactions.

However, in order to benefit from new aerosol datasets improvements in regional NWP models are required. Technical changes are needed to introduce external three-dimensional (hereafter denoted as 3D) aerosol load data into these models in near real-time (n.r.t. hereafter). More detailed information on the optical properties of aerosols such as the aerosol optical depth (hereafter AOD) or mass extinction coefficient (ME), single-scattering albedo (SSA) and asymmetry parameter (ASY) is needed combined with the improved aerosol concentration data.

The work presented in this paper expands on the studies by [12,13]. Three radiation schemes available in the shared ALADIN-HIRLAM Numerical Weather Predication system [18] (hereafter the ALADIN-HIRLAM NWP system) were compared using a single-column model approach [12]. Observed AODs at different SW wavelengths were used to constrain the radiative transfer parametrizations in a Russian wildfire case in summer 2010. The aerosol load (AOD at the 550 nm wavelength, hereafter AOD550) was found to be the most important factor influencing SW radiation fluxes at the Earth's surface. The radiation schemes produced realistic results only when observation-based wavelength-dependency of AOD, SSA and ASY were taken into account. In particular, it was shown that the SW broadband AOD differs from AOD550.

The impact of aerosols on SW radiation fluxes and near-surface temperatures was studied in 3D climate and NWP model simulations of ALADIN-HIRLAM [13]. That study showed that updating the input aerosol climatology from the default Tegen AOD550 climatology [19] to a simplified CAMS-based AOD550 climatology did not lead to significant changes in the climate simulation results. n.r.t 3D CAMS aerosol concentrations were included in a Saharan dust case study. ME coefficients at 550 nm were used to convert the MMR in the n.r.t. dataset to AOD550. Although the AOD550 values were updated

based on n.r.t. data, the default wavelength-dependencies for AOD, SSA and ASY were still used. The results showed good agreement with local temperature and radiation observations despite the simplified treatment of the aerosol IOPs, indicating that the aerosol load had the largest impact.

In this paper we report on the next steps in the renewal of the aerosol radiative transfer parametrizations in ALADIN-HIRLAM. Aerosol-wise, the system uses default Tegen climatologies [19] of AOD550 of land, sea, desert, urban and sulfate aerosols and the following aerosol IOPs: AOD wavelength-scaling factor, SSA and ASY based on [20,21]. Our upgrades involve the combination of updated IOPs (ME, SSA and ASY for 11 aerosol species at 30 wavelengths) from ECMWF [6,24] and aerosol concentrations from the CAMS reanalysis [4] or CAMS n.r.t. data [5].

The single column version of ALADIN-HIRLAM, known as MUSC [22], was used to carry out the various sensitivity tests. Input atmospheric and surface profiles, needed for the single-column experiments, were extracted from 3D simulations done using the HARMONIE-AROME [23] configuration of the ALADIN-HIRLAM system. We analyse aerosol SW and LW transmission and absorption characteristics from a range of MUSC experiments in detail. We have introduced the updated aerosol optical properties into the HIRLAM broadband radiation scheme [25,26], the simplest radiation scheme available in HARMONIE-AROME. Using HLRADIA, we then tested the impact of aerosols on the radiative fluxes and atmospheric temperature tendencies due to radiation.

Our aim is to understand the importance of realistic estimations of the distributions of different aerosol species and accurate IOPs of these species for the calculation of aerosol radiative transfer. In this study we focus on the direct radiative effect of aerosols using clear-sky cases so that the interactions between cloud-microphysics, precipitation and radiation are excluded. Comparisons with observations have not been made. Instead, sensitivities and uncertainties under real atmospheric conditions are considered. Comparisons with observations will be carried out in the next phase using the full ALADIN-HIRLAM NWP system rather than MUSC.

The paper is organised as follows: Section 2 provides a description of aerosol radiative transfer in the ALADIN-HIRLAM NWP system. Section 3 describes and presents the results of the MUSC experiments. The results are summarised and discussed in Section 4. Finally, information about the ALADIN-HIRLAM NWP system, its radiation parametrizations and the CAMS aerosol data used in the experiments is provided in Section 5.

2. Aerosol radiative effects in the ALADIN-HIRLAM NWP System

In this section we summarise the main features of the parametrization of aerosol radiative effects in the ALADIN-HIRLAM NWP system, in particular within HARMONIE-AROME. Section 5 explains the ALADIN-HIRLAM NWP system and its radiation parametrizations in more detail.

Radiation schemes estimate the radiative heating in the atmosphere due to the vertical divergence of the net LW (terrestrial) and net SW (solar) radiation fluxes in an NWP model. This heating is a source term in the thermodynamics equation in the model and influences atmospheric temperatures and the evolution of clouds. At the surface, radiation parametrizations provide the model with downward (LWDS, SWDS; the D refers to downwards and the S to surface) and upward LW and SW radiation fluxes. At the top of the atmosphere (TOA), the outgoing fluxes are given (LWUT, SWUT; the U refers to upward and T refers to top). The surface fluxes are part of the surface energy balance and a lower boundary condition for the calculation of atmospheric radiation transfer. At the TOA, downwelling SW radiation defines the upper boundary condition for radiation parametrizations. Surface properties such as temperature, albedo and emissivity are also required as input. In terms of aerosols, the radiation schemes include parametrization of the direct radiative effect of aerosols due to absorption and scattering in the SW part of

Preprints (www.preprints.org) | NOT PEER-REVIEWED | Posted: 17 January 2020 doi:10.20944/preprints202001.0183.v1

the spectrum and absorption/emission in the LW. The indirect radiative effect of aerosols, which is related to the cloud-aerosol interactions, is currently not included in HARMONIE-AROME.

In the ALADIN-HIRLAM NWP system the direct radiative impact of aerosols is treated by the radiation parametrizations which use a climatology of AOD550 as input. Monthly climatologies of four classes of tropospheric AOD550 (land, sea, desert and urban where the 'land' classification includes sulfates) based on [19] are used by default. In addition, stratospheric sulfates and volcanic dust are accounted for using assumed background values. The six AOD550 fields are distributed vertically using the assumed exponential profiles of Tanré [27] in the same way as described by [6]. Aerosol IOPs, namely the relation of AOD to AOD550 (i.e. the AOD factor), the SSA and ASY, of the 6 aerosol species are prescribed for 6 SW and 6 LW intervals in the default IFSRADIA radiation scheme. Two broadband radiation schemes, HLRADIA and ACRANEB, available for experimenting within HARMONIE-AROME, have been adapted to use the default AOD550 climatology as input. Section 5.2 contains references and details for the three radiation schemes.

We used HLRADIA for the single-column study of the sensitivity of radiation fluxes to aerosol concentration and optical properties. The original HLRADIA scheme [26] estimates the impact of aerosols on radiation by applying constant coefficients to represent SW absorption and scattering and LW absorption and emission. Thus no climatological or other gridded aerosol load data are used. The treatment of aerosol data and IOPs by HLRADIA was renewed in the Enviro-HIRLAM modelling environment using GADS/OPAC data [20,21] and software as suggested in [2]. The aerosol optical properties are derived from GADS/OPAC ME, SSA and ASY and then remapped to the default AOD550 input of 6 aerosol species and spectrally averaged for the single SW and LW bands. Relative humidity from the model is taken into account. The resulting broadband optical depths of the aerosol mixture are scaled using a delta-Eddington factor [28] in the form 1 - SSA x $(ASY)^2$. This AOD550-based HLRADIA were first applied in HARMONIE-AROME experiments in [12] for the 2010 Russian wildfire case study, involving only SW effects.

For the current study we have adapted HLRADIA to use CAMS aerosol MMR data (unit kg/kg) combined with up-to-date aerosol IOPs from ECMWF as input instead of AOD550. In this MMR-based approach, monthly 2D climatologies based on reanalysis data [4,24] or 3D n.r.t. data [5] can be used. For our purposes, data for 11 aerosol species were extracted: 3 size bins of hydrophilic sea salt (SS) aerosols; 3 size bins of hydrophobic mineral (desert) dust (DD) aerosols, hydrophilic and hydrophobic organic matter (OM); hydrophilic and hydrophobic black carbon (BC) and hydrophilic sulfate (SU). SS corresponds approximately to the Tegen 'sea' aerosol category, DD to 'desert', OM to 'land' without sulfates and BC to 'urban' aerosols. Updated exponential functions [6] were applied to distribute the 2D climatological data vertically on model levels where needed. The CAMS data and ECMWF IOPs are described in more detail in Section 5.3.

The vertical distribution of aerosols and the atmospheric state, mainly the humidity distribution, influences the profiles of the radiative transfer properties of the aerosols throughout the atmosphere. However, HLRADIA treats atmospheric layers in a simplified way, and also the way to take the aerosol properties into account involves averages. Aerosol SW and LW transmission and LW absorption are calculated for three atmospheric layers - a layer above the clouds, in the clouds and below the clouds. Multiple cloud layers are treated as a single thick layer ignoring the clear-sky layers between them. In cases without clouds, the aerosol transmission and absorption are calculated for the entire atmospheric column.

The downwelling SW flux at the top of the cloud or at the surface is estimated by taking into account the aerosol transmission from the TOA to the model level in question. Only the SW absorption by aerosols is calculated in a detailed way, namely level by level using the absorption optical depth from the TOA to each level. LW heating is calculated at each model level using the average above/in/below-cloud

Preprints (www.preprints.org) | NOT PEER-REVIEWED | Posted: 17 January 2020 doi:10.20944/preprints202001.0183.v1

transmission and absorption. The averages are obtained by integrating the model-level AOD, SSA and ASY in the column between the top and bottom of each of the three layers but from TOA to surface in the clear-sky conditions.

To summarise, in this study we test three different flavours of HLRADIA parametrizations of aerosol radiative transfer: the original, the AOD550-based and the MMR-based. For the comparison, some results of the AOD550-based IFSRADIA and ACRANEB are also shown.

3. Results

In this section the experiments are defined in Section 3.1. As a starting point, results of tests done using three radiation schemes and the default AOD550-based aerosol parametrizations are compared in Section 3.2. In the following sections we used the HLRADIA radiation scheme for the detailed study of the impact of different climatological and n.r.t. aerosol input data and IOPs. The results of two case studies based on realistic aerosol data are discussed in Sections 3.3 and 3.4 and the results of sensitivity studies using artificial aerosol data are given in Section 3.5.

3.1. Experiments

Table 1 summarises the series of MUSC experiments carried out in this study. Further information about the MUSC is given in Section 5.1. The input data (aerosols, and atmospheric and surface state) for these experiments were taken from 3D HARMONIE-AROME experiments for two locations: Lake Ladoga in Russia for the 19th of April 2019 and Badajoz in Spain for the 21th of February 2017. The incoming solar radiation at the top of atmosphere was 895 Wm^-2 over Badajoz and 778 Wm^-2 over Ladoga. The surface albedo was 0.07 in Badajoz (a water surface assumed) and 0.37 over Lake Ladoga (the lake was assumed to be partly frozen). The LW emissivity of the surface was 0.97 for both cases.

Experiments were done using both 3D n.r.t. and 2D climatological aerosol MMR data. Experiment names starting with C used climatological aerosol input data while those starting with N used n.r.t. data, 2 denotes vertically integrated (2D) aerosol data and 3 denotes column (3D) data. Sensitivity tests of MMR and AOD series used modified aerosol inputs, combined with the atmospheric state at Lake Ladoga.

Table 1. Single-column experiments

Experiment	Aerosol load (AOD or MMR)	Aerosol IOPs	Note
No aerosol input			
ZERO	none	none	all aerosols excluded
HSA	Savijarvi coefficients	not specified	aerosols assumed constant [26]
MMR input			
CMMR2	climatological total-column MMRs	IOPS [24] for 11 sp at 30 wl and 10 RH	2D CAMS MMR climatology as in [24]
NMMR3	n.r.t. MMR profiles	IOPS [24] for 11 sp at 30 wl and 10 RH	3D CAMS n.r.t. MMR data as in [13]
NMMR2	total-column MMRs from NMMR3	IOPS [24] for 11 sp at 30 wl and 10 RH	impact of vertical distribution
MMR series	like NMMR2 but modified MMRs	IOPS [24] for 11 sp at 30 wl and 10 RH	sensitivity to aerosol concentration
AOD550 input			
CAOD2	climatological total-column AOD550	IOPs [20,21] for 6 sp at 12 wl	2D Tegen climatology [19]
NAOD2	total-column AOD550 from NMMR3	IOPs [20,21] for 6 sp at 12 wl	for comparison of optical properties
AOD series	like NAOD2 but modified AOD550	IOPs [20,21] for 6 sp at 12 wl	sensitivity to optical properties

'sp' refers to aerosol species, 'wl' refers to wavelength and 'RH' to relative humidity. MMR and AOD refer to mass mixing ratio and AOD550 input, respectively. IOP stands for aerosol inherent optical properties that consist of ME, SSA and ASY in MMR experiments, and AOD scaling factor, SSA and ASY in AOD550 experiments.

The ZERO experiments do not include aerosols. Experiment HSA uses constant coefficients for aerosol radiative transfer [25]. CAOD2, which is the reference experiment, uses monthly climatological values of

 doi:10.20944/preprints202001.0183.v1

AOD550 for land (OM + SU), sea (SS), desert (DD) and urban (BC) aerosols. The CMMR2 experiments use vertically integrated climatological MMRs of 11 species, given on the same 2.5 degree resolution global horizontal grid as the climatological AOD550 data. These data are based on CAMS interim reanalysis output for 2003-2011, and IOPs applied therein [24]. No background aerosols are added when MMR data are used.

The NMMR3 experiment uses 3D n.r.t. CAMS aerosol data. Output of this MUSC experiment included vertically integrated MMR for the 11 species, that was used as input for experiment NMMR2, and AOD550 which was used as input for the NAOD2 experiment. Thus, the experiments NMMR3 and NMMR2 differ only with respect to the vertical distribution of aerosol MMR whereas experiments NMMR2 and NAOD2 differ with respect to the optical properties. The sensitivity experiment series MMR and AOD differ in similar ways to NMMR2 and NAOD2 but only a single aerosol species is included in each experiment.

3.2. Comparison of three radiation schemes using AOD550 input

In this section we present an example of radiative heating profiles extracted from the first time step of the MUSC experiments for both the Badajoz and Ladoga locations. Figure 1 shows the comparison of results for the IFSRADIA, HLRADIA and ACRANEB radiation schemes. The schemes are denoted as "i", "h" and "a" in the figures shown. A summary of these radiation schemes is given in Section 5.1. Cases with no aerosol input (ZERO, HSA) and both climatological (CAOD2) and n.r.t. (NAOD2) AOD550 input are shown. CAOD2 with IFSRADIA is the default set-up in HARMONIE-AROME. The result of HLRADIA using 3D n.r.t MMRs and updated aerosol IOPs, that represents the aerosol renewal suggested in this study is also shown for preliminary comparison.

When aerosols are excluded (ZERO), when original coefficients are used (HLRADIA with HSA) or when the climatological aerosol load is assumed (CAOD2) all schemes show similar SW heating rates for Badajoz, with a maximum of approximately 2.5 K/day in the upper troposphere. The SW heating rate increases by 2 to 3 degrees/day in the lower troposphere, most by HLRADIA, when an estimated n.r.t. aerosol load is included in terms of AOD550 (NAOD2 curves in Figure 1a). The HLRADIA scheme shows a smoother LW profile with more/less cooling in the lower/upper troposphere than IFSRADIA and ACRANEB, most likely due to its simplified LW radiation parametrization (Figure 1c). The inclusion of aerosols makes almost no difference to the LW cooling rates shown by each of the three schemes. The total temperature tendency due to radiation is determined by the sum of SW and LW contributions (Figure 1e), which tend to balance each other. For Ladoga (Figures 1b,d,f), the differences between the schemes due to aerosols are smaller because of the smaller aerosol load and different composition. Note that the n.r.t. data used for Badajoz is for a case involving a Saharan dust intrusion while the Ladoga case represents normal background conditions.

The corresponding radiation fluxes at the surface and at the top of atmosphere (TOA) are shown in Table 2. All schemes give similar results when aerosols are excluded, with the exception of LW fluxes when HLRADIA is used. Outgoing LWUT (positive upwards) is larger and LWDS (positive downwards) is smaller for HLRADIA. Large LWUT means that also the net radiation (the sum of SW and LW net fluxes) at TOA (denoted as NETT in Table 2) is smaller when HLRADIA is used. Overestimation of the atmospheric LW absorption by HLRADIA was reported in [25] in experiments where aerosols were excluded.

SWDS decreases when the climatological (CAOD2) or n.r.t. (NAOD2) AOD550 is included in the the experiments. The decrease is largest for HLRADIA. SWUT decreases somewhat when IFSRADIA or ACRANEB are used with the small aerosol load over Ladoga but it increases when HLRADIA is used for the same case. Over Badajoz, where the load is larger and dominated by desert dust, all experiments show an increase in SWUT, again with the largest increase when HLRADIA is used. In HLRADIA SW net flux is diagnosed from the SW heating profile, where by default scattering by aerosols does not bear

Preprints (www.preprints.org) | NOT PEER-REVIEWED | Posted: 17 January 2020 doi:10.20944/preprints202001.0183.v1

an influence. The diagnostic values shown in Table 2 were now corrected so that about half of the SW radiation scattered by aerosol particles was added to the net SW flux at each model level. This uncertainty in the diagnostics means that SWUT and NETT by HLRADIA are not really suitable for comparison to the other radiation schemes for cases where aerosols are included. The LW fluxes are less sensitive to aerosols for all radiation schemes.

Table 2. Radiative fluxes at the surface and top of atmosphere

	Badajoz				Ladoga					
Scheme	**SWDS**	**SWUT**	**LWDS**	**LWUT**	**NETT**	**SWDS**	**SWUT**	**LWDS**	**LWUT**	**NETT**
IFSRADIA										
ZERO	692	95	282	253	547	623	256	240	226	298
CAOD2	680	97	283	253	545	588	244	241	225	310
NAOD2	556	119	284	253	523	580	243	241	226	310
HLRADIA										
ZERO	693	89	257	310	535	622	255	206	268	281
HSA	656	124	265	307	507	593	273	214	266	271
CAOD2	636	140	258	308	447	550	281	207	267	231
NAOD2	512	148	269	304	446	539	280	207	267	232
NMMR3	534	147	286	293	454	580	263	208	266	249
ACRANEB										
ZERO	695	91	287	258	546	624	255	244	228	295
CAOD2	677	100	287	258	545	586	250	245	228	301
NAOD2	551	132	288	257	523	577	250	245	228	301

SWDS and LWDS are the downwelling SW and LW fluxes at the surface, positive downwards. SWUT and LWUT are the outgoing SW and LW fluxes at TOA, positive upwards. NETT is the net SW + LW radiation, positive downwards. Unit of all fluxes is Wm^{-2}. SW downwelling flux at TOA is 895 Wm^{-2} for Badajoz and 779 Wm^{-2} for Ladoga.

Figure 1 and Table 2 also include results from experiment NMMR3 done using HLRADIA with the CAMS aerosol data and ECMWF optical properties (blue crosses in Figure 1). The SW and total heating rates (Figure 1, top and bottom rows) differ from the other results, in particular for the lower troposphere in the Badajoz case. Here the lower tropospheric SW heating (Figure 1a) decreases by approximately 2 K/day compared to NAOD2. For the case of LW heating rates the differences are small. SWDS from HLRADIA increases compared to NAOD2 both at Badajoz and Ladoga. At Ladoga SWUT also increases while at Badajoz the LW fluxes are affected (Table 2).

From here on we continue with more detailed analysis of aerosol radiative transfer using the HLRADIA scheme only. For consistency, and bearing in mind the differences between the results of the three radiation schemes, we will compare HLRADIA MMR-based experiments to HLRADIA AOD-based experiments.

3.3. Comparisons over Lake Ladoga and in Badajoz using HLRADIA

Total-column diagnostics of the aerosol radiative transfer over Badajoz and Ladoga are presented in Table 3 for all of the experiments except ZERO and HSA where external aerosol data were not used. In terms of column-integrated AOD550, the largest aerosol load (0.544) was present in the NMMR3 and NMMR2 experiments, where there was a significant intrusion of desert dust aerosols and new IOPs were used. The smallest AOD550 for the Badajoz case (0.085, CAOD2) resulted from the use of the AOD550 climatology and prescribed optical properties. The broadband SW optical depths (TAUSW) are smaller than the AOD550 values in all experiments at both locations. The total-column MMR of all aerosols combined (TOTMMR) is shown in Table 3 for the MMR-related experiments. TOTMMR is not directly

Preprints (www.preprints.org) | NOT PEER-REVIEWED | Posted: 17 January 2020 doi:10.20944/preprints202001.0183.v1

correlated with the optical depths of the aerosol mixture because the optical properties are specific to each aerosol species.

The SW transmission (SWTRAN) was smallest over Badajoz (0.78) in the NMMR3 and NAOD2 experiments and largest (0.98) in CMMR2. The values of SWABS, the diagnostic vertically integrated SW absorption, are less than 10% of the transmission values. Aerosol SW scattering is given by 1 - SWTRAN - SWABS. Maximum scattering (0.16) occurred in the Badajoz experiment NMMR3. The LW optical depths are typically at least an order of magnitude lower than the SW optical depths. The lowest value of LW transmission (LWTRAN) was 0.90 in the NMMR2 and NMMR3 experiments for Badajoz. Experiment NMMR2 showed the largest LW absorption (0.08) and scattering (0.02).

Table 3. Aerosol SW and LW transfer

EXPERIMENTS BASED ON AEROSOL CONCENTRATION AND OPTICAL PROPERTIES INPUT

Experiment	AOD550[1] unitless	TOTMMR g/m^2	TAUSW unitless	SWTRAN (0...1)	SWABS (0...1)	TAULW unitless	LWTRAN (0...1)	LWABS (0...1)
Badajoz								
CMMR2	0.104	0.239	0.076	0.98	0.005	0.018	0.98	0.019
NMMR3	0.544	0.521	0.465	0.78	0.063	0.077	0.90	0.086
NMMR2	0.544	0.521	0.471	0.85	0.066	0.077	0.90	0.082
Ladoga								
CMMR2	0.087	0.056	0.054	0.98	0.009	0.011	0.99	0.012
NMMR3	0.204	0.050	0.104	0.93	0.031	0.006	0.99	0.008
NMMR2	0.204	0.050	0.111	0.94	0.004	0.007	0.99	0.008

EXPERIMENTS BASED ON AOD550 INPUT

Experiment	AOD550[2] unitless	TAUSW unitless	SWTRAN (0...1)	SWABS (0...1)	TAULW unitless	LWTRAN (0...1)	LWABS (0...1)
Badajoz							
CAOD2	0.085	0.073	0.97	0.012	0.001	1.00	0.001
NAOD2	0.574	0.550	0.78	0.111	0.036	0.95	0.036
Ladoga							
CAOD2	0.187	0.159	0.93	0.031	0.002	1.00	0.002
NAOD2	0.242	0.203	0.91	0.038	0.001	1.00	0.001

The total column AOD550 [1] is a diagnosed output of the experiments, [2] is an input value and includes an assumed stratospheric (sulphate) and tropospheric background AOD550 of ≈ 0.04.

Average characteristics of aerosol radiative transfer due to all species combined: AOD550 - total aerosol optical depth at 550 nm, TOTMMR - vertically integrated total aerosol MMR, TAUSW - broadband average SW aerosol optical depth, SWTRAN - aerosol SW transmission coefficient, SWABS - aerosol SW absorption coefficient, TAULW - broadband average LW aerosol optical depth, LWTRAN - aerosol LW transmission coefficient, LWABS - aerosol LW absorption coefficient.

The NMMR3 and NMMR2 experiments use the same n.r.t. MMR data, with the difference being how the aerosols are distributed vertically on model levels. This leads to different SWTRAN values, 0.78 for NMMR3 and 0.85 for NMMR2 in Badajoz. The reason is related to the vertical distribution of the different aerosol species and the resulting optical properties. We will analyse this in more detail in Section 3.4.

Firstly, we will consider the net LW and net SW radiative flux profiles for Badajoz and Ladoga (Figure 2). At Badajoz the maximum difference in the net SW flux at the surface is 170 W/m^2 or 26% for the ZERO (no aerosol) experiment compared to NAOD2 which is almost the same as for NMMR3 (Figure 2a). This difference is of the same order of magnitude as the maximum differences seen in 3D HARMONIE-AROME experiments [13] for the same case study. The NMMR3 and NAOD2 experiments involving n.r.t. data show the smallest net SW fluxes at Badajoz while those based on climatological

Preprints (www.preprints.org) | NOT PEER-REVIEWED | Posted: 17 January 2020 doi:10.20944/preprints202001.0183.v1

aerosol (CMMR2D, CAOD2D) are the largest. The net SW fluxes for experiment NMMR2 appears between those from the n.r.t experiments and the climatological experiments. The maximum difference in SWNET between the NAOD2 and ZERO experiments over Ladoga is smaller, 50 W/m^2 or 13% (Figure 2b). The value of SWNET that is closest to that from the ZERO experiment is for the NMMR3 experiment

The net LW flux is similar in all experiments over Ladoga (Figure 2d), while for Badajoz the NMMR2 and NMMR3 experiments, which show the lowest LW transmission (Table 3), have the smallest negative (i.e. upward) net LW fluxes at each level in the atmosphere (Figure 2c).

Table 4 gives a summary of the vertically integrated broadband aerosol optical properties for the aerosol mixture used in the experiments. These were estimated from prescribed IOPs and atmospheric humidity profiles (see Section 2). Estimates of the scaled broadband SW and LW optical depths $TAUSW_s$ and $TAULW_s$, single scattering albedos SSASW and SSALW and asymmetry factors ASYSW and ASYLW are shown. The single-scattering albedo is a ratio of scattering to total extinction and varies from 0 for a fully absorbing medium, to 1 for a fully scattering medium. Asymmetry factor represents the fraction of forward scattering to total scattering. Remember that the optical depths are scaled by the a factor 1 - SSA x $(ASY)^2$ when calculating the SW and LW absorption and scattering by aerosols within HLRADIA. $TAUSW_s$ and $TAULW_s$ shown in Table 4 have been calculated from the vertically integrated SSA and ASY. Such an estimate does not exactly represent the scaling that is done at each model level because of the nonlinearity of the scaling factor.

For the Badajoz and Ladoga cases, SSASW varies from 0.78 (NMMR3 for Badajoz and Ladoga) to 0.96 (CMMR2 for Badajoz). SSALW varies between 0.26 (Ladoga, NMMR2) and 0.39 (Ladoga, NAOD2). ASYSW varied less and lay within the range 0.63-0.71. For ASYLW the AOD550-based experiments show values of around 0.2 while in the experiments based on MMR and new IOPs the values vary from 0.4 to 0.66. SSA and ASY differences between Badajoz and Ladoga reflect the different aerosol compositions at these locations.

Preprints (www.preprints.org) | NOT PEER-REVIEWED | Posted: 17 January 2020 doi:10.20944/preprints202001.0183.v1

Table 4. Optical properties of aerosol mixtures

EXPERIMENTS BASED ON AEROSOL CONCENTRATION AND OPTICAL PROPERTIES INPUT

Experiment	$TAUSW_S$ unitless	SSASW (0...1)	ASYSW (0...1)	$TAULW_S$ unitless	SSALW (0...1)	ASYLW (0...1)
Badajoz						
CMMR2	0.039	0.96	0.71	0.016	0.38	0.56
NMMR3	0.318	0.78	0.64	0.070	0.33	0.50
NMMR2	0.272	0.92	0.68	0.073	0.36	0.40
Ladoga						
CMMR2	0.030	0.92	0.70	0.009	0.37	0.57
NMMR3	0.073	0.76	0.63	0.005	0.27	0.66
NMMR2	0.074	0.82	0.64	0.006	0.26	0.66

EXPERIMENTS BASED ON AOD550 INPUT

Experiment	$TAUSW_S$ unitless	SSASW (0...1)	ASYSW (0...1)	$TAULW_S$ unitless	SSALW (0...1)	ASYLW (0...1)
Badajoz						
CAOD2	0.047	0.90	0.63	0.001	0.37	0.22
NAOD2	0.362	0.86	0.63	0.035	0.39	0.21
Ladoga						
CAOD2	0.104	0.88	0.63	0.002	0.36	0.20
NAOD2	0.132	0.89	0.63	0.001	0.28	0.18

Vertically integrated broadband aerosol optical properties for all species combined: $TAUSW_S$ - scaled SW aerosol optical depth, SSASW - SW single-scattering albedo, ASYSW - SW asymmetry factor, $TAULW_S$ - scaled LW aerosol optical depth, SSALW - LW single-scattering albedo, ASYLW - LW asymmetry factor. TAUSW and TAULW were copied from Table 3.

Figure 3 shows the vertical distribution of aerosol MMRs for the CMMR2, NMMR3 and NMMR2 experiments. The vertically integrated MMR input for CMMR2 is based on CAMS interim reanalysis 2003-2011 [4] as used by [24] while the column data for NMMR3 was extracted from the CAMS n.r.t. database (see Section 5.3 for the details of CAMS data). Input to NMMR2 was extracted from diagnostic output of NMMR3. The 2D aerosol MMRs were expanded vertically by using exponential profiles specific to the five aerosol types according to [6].

Figures 3a and 3b show the different aerosol compositions over Badajoz and Ladoga. At Badajoz a layer of desert dust is seen between 900 and 700 hPa where the maximum aerosol load reaches 0.1 $\mu g/kg$ on several of the lower tropospheric levels. The load by the other species is at least one order of magnitude smaller. Over Ladoga, according to the CAMS n.r.t. data, OM and SU dominate but their concentrations only reach a maximum of 0.01 $\mu g/kg$ around the 850 hPa level. Figures 3c and 3d show the resulting aerosol concentration profiles when the n.r.t. data were first vertically integrated and then redistributed using the assumed exponential functions [6]. The dominance of DD at Badajoz and OM and SU over Ladoga is clearly seen. Figures 3e and 3f show the climatological (CAMS interim reanalysis) distributions, where at Badajoz and over Ladoga the largest component is SS, followed by DD with a concentration that is an order of magnitude smaller. Such composition seems somewhat unrealistic especially for Ladoga, but might be explained by the coarse resolution of the input data (2.5 x 2.5 degrees on a latitude-longitude grid, interpolated to the HARMONIE-AROME grid of 2.5 x 2.5 km). Overall, the climatological aerosol concentrations are small at both locations.

The composition of the aerosol mixture and the IOPs of each aerosol type determine the broadband optical properties. The vertical distributions of aerosol species influence the profiles of TAU, SSA and ASY. The atmospheric humidity profile modifies the optical properties of hydrophilic aerosol species. The

Preprints (www.preprints.org) | NOT PEER-REVIEWED | Posted: 17 January 2020 doi:10.20944/preprints202001.0183.v1

broadband SW and LW optical properties are illustrated in Figure 4 and Figure 5 for the Badajoz and Ladoga cases.

According to n.r.t. data (experiment NMMR3) TAUSW reaches maximum values above the 850 hPa level both at Badajoz and over Ladoga (Figure 4). When exponential profiles are used (experiment NMMR2), the distribution broadens in the vertical. The climatological distribution (CMMR2) shows smaller values especially over Badajoz. The influence of aerosol composition - hydrophobic desert dust dominates over Badajoz, hydrophilic sulfate and organic matter dominate over Ladoga - shows up in the NMMR2 profiles where the smooth exponential curve breaks for Ladoga due to vertical humidity variations. The SWTAUA profiles are smoother because the strongest absorbing components are hydrophobic and the maxima are located higher than those of total TAUSW. SSASW and ASYSW distributions show differences between experiments and vertically but the range of variations is smaller.

The LW optical depth (Figures 5a and 5b) is clearly smaller than the SW optical depth as was already shown in Table 4. Similar features and variations as in the SW profiles are seen in the vertical distributions. The range of variations for SSALW (Figures 4d and 4d) and ASYLW (Figures 4e and 4f) is however larger than for SSASW and ASYSW.

3.4. An example of radiative heating at Badajoz

Figure 6a shows the SW radiative heating for all of the experiments included in Table 3. The heating suggested by the NMMR2 and NAOD2 experiments is most pronounced at the lowest model levels. In the layer 900-500 hPa the NMMR2 experiment shows less heating than NMMR3 and NAOD2. These differences are related to the different SWTRAN values found in Table 3 and mentioned in Section 3.3. For NMMR3 and NMMR2 the TAUSW values do not differ by much. However, SSASW is different, 0.78 for NMMR3 and 0.92 for NMMR2 (Table 4). This means that in NMMR3 the aerosols are more absorbing while in NMMR2 the aerosol scattering is higher. Indeed, the scaled $TAUSW_s$ values are larger (0.318) for NMMR3 than for NMMR2 (0.272), which directly influences the values of SWTRAN. (The unscaled TAUSW is slightly smaller for NMMR3 (0.465) than for NMMR2 (0.471) as shown in Table 3). Where does the difference in SSASW come from?

The vertically integrated aerosol load in terms of MMRs is by definition the same for NMMR3 and NMMR2 (Table 4). For NMMR3 a 3D distribution of aerosol data obtained from CAMS is used (Figure 3a) while for NMMR2 exponential vertical profiles are assumed (which is why they appear as straight lines on the log-log plot in Figure 3c). We can see differences close to the surface and in the middle troposphere (differences in heating rates in Figure 6a). The differences in the upper troposphere are insignificant due to small aerosol loads at those levels.

Vertical distribution of the aerosol mass is reflected in the distribution of the optical properties. In particular, the SWSSA values in NMMR3 above the dust layer are small, which indicates strong absorption (Figure 4e). Indeed, the absorption optical depth (SWTAUA) has a second maximum at those levels (Figure 4c). Figure 3a shows that above the 600 hPa level, the concentration of all aerosols other than DD is larger in NMMR3 than in NMMR2. Which of them causes the middle troposphere difference? Figure 6b shows what happens when black carbon is excluded from the experiments. Most notably, heating profile of NMMR2 changes and becomes more similar to NMMR3. The SW heating rate in each of the experiments NMMR2, NMMR3 and NAOD2 decreases somewhat. The second maximum in SWTAUA which is above the NMMR3 dust layer disappears (not shown) and the SWTRAN values become 0.86 and 0.88 for NMMR3 and NMMR2 respectively, compared to previous values of 0.78 and 0.85.

These differences are not large, but the example shows the interaction between the distribution of different aerosol species and the optical properties. It suggests that it is important to account for such details when the aerosol loads of some species are substantial. In particular, the example shows a possible

 doi:10.20944/preprints202001.0183.v1

role of the strongly absorbing BC. In addition, from a practical point of view the example demonstrates the power of single-column experiments as a tool for diagnosing and interpreting experiment results.

3.5. Species-specific sensitivity tests

In this section we focus on the results of the MMR and AOD series of experiments described in Table 1 with a focus on the impact of the different aerosol species. For the MMR series of experiments 11 bins of total column MMR were combined to 5 classes : SS, DD, OM, BC and SU so that the resulting diagnostic AOD550 for each of the combined species was 0.5. The ratios within each class (e.g. between the three size bins of DD or hydrophilic and hydrophobic OM) were retained and the new IOPs were applied to the original 11 species when running the experiments. For the AOD experiments AOD550 = 0.5 was assigned to each of the Tegen aerosol categories: sea, desert, land, urban+sulfate. The default background values for stratospheric and tropospheric aerosols were not modified. The default prescribed IOPs were used in the AOD series experiments. The 5 aerosol classes in the MMR and AOD experiments are assumed to roughly correspond to each other.

The SW transmission (SWTRAN=0.56) was smallest for the case of BC in the MMR-BC experiment (Table 5). The transmission was larger (0.79) in the AOD-BC experiment where AOD550 input was combined with old IOPs. This large difference is thus related to different optical properties. The values of SWABS diagnosed from MMR-BC suggest that the absorption capability of BC is at least an order of magnitude larger than that of the other species. Absorption by BC reduces SWTRANS even though the broadband TAUSW is smaller (0.367) in the MMR-BC experiment than in AOD-BC (0.448). This is because the scaled TAUSW_s (Table 6) is larger (0.365) in MMR-BC than in AOD-BC (0.309). In AOD-BC scattering (1-SWTRAN-SWABS) is 0.11 but in MMR-BC it is 0.06. The situation is the opposite for the more scattering SU or DD aerosols. For example, SWTRAN for DD is 0.84 in MMR-BC but 0.76 in AOD-DD, and in the latter SWABS is 5 times the former. This can also explain the differences between the NAOD2 and NMMR2 experiments at Badajoz, where the DD aerosol dominates (Figure 3) and SWTRAN is clearly larger in NMMR2 (0.85) than in NAOD2 (0.78) (Table 3).

Preprints (www.preprints.org) | NOT PEER-REVIEWED | Posted: 17 January 2020 doi:10.20944/preprints202001.0183.v1

Table 5. SW and LW aerosol properties by aerosol category

EXPERIMENTS BASED ON AEROSOL CONCENTRATION AND OPTICAL PROPERTIES INPUT

Experiment	AOD550[1] unitless	TOTMMR g/m^2	TAUSW unitless	SWTRAN (0...1)	SWABS (0...1)	TAULW unitless	LWTRAN (0...1)	LWABS (0...1)
MMR series								
MMR-SS	0.5	0.948	0.257	0.95	0.004	0.062	0.93	0.059
MMR-DD	0.5	0.775	0.564	0.84	0.025	0.096	0.88	0.104
MMR-OM	0.5	0.160	0.287	0.86	0.067	0.026	0.97	0.027
MMR-BC	0.5	0.037	0.367	0.56	0.400	0.015	0.98	0.025
MMR-SU	0.5	0.080	0.251	0.90	0.017	0.009	0.99	0.015

EXPERIMENTS BASED ON AOD550 INPUT

Experiment	AOD550[2] unitless	TAUSW unitless	SWTRAN (0...1)	SWABS (0...1)	TAULW unitless	LWTRAN (0...1)	LWABS (0...1)
AOD series							
AOD-SS	0.54	0.523	0.90	0.007	0.006	0.99	0.004
AOD-DD	0.53	0.545	0.76	0.125	0.049	0.94	0.050
AOD-OM	0.54	0.450	0.81	0.084	0.002	1.00	0.003
AOD-BC	0.54	0.448	0.79	0.104	0.002	1.00	0.003
AOD-SU	0.54	0.450	0.81	0.084	0.002	1.00	0.003

Total-column AOD550 [1] is diagnosed output of the experiments, [2] is an input value and includes assumed stratospheric (sulphate) and tropospheric background AOD550 ≈ 0.04.

Aerosol categories: SS - sea salt, DD - desert dust, OM - organic matter, BC - black carbon, SU - sulphate.

The smallest LWTRANS values occurred in the DD MMR-DD (0.88) and AOD-DD (0.94) experiments because of the dominance of coarse particles within this category of aerosols. The results confirm that our parametrizations work as expected but also show that the MMR-based and AOD-based approaches influence in the LW part of the spectrum. Nevertheless, the impact of the difference on LW radiative fluxes is minor.

Figure 7 shows LW and SW net radiative flux profiles for the MMR and AOD series of experiments. The maximum difference in SW fluxes compared to the ZERO aerosol experiment is somewhat smaller (ca. 100 Wm^{-2}) in the AOD experiments than in the MMR experiments (ca. 200 Wm^{-2}). The most striking feature of the MMR experiments is the strong impact of BC on the net SW flux near the surface. The impact is smaller in the AOD experiments although in both cases the vertically integrated AOD550 is approximately 0.5. In both cases, the MMR or AOD550 was distributed vertically using the same exponential function. However, the IOPs and their wavelength and humidity dependencies are different, and this leads to different broadband optical properties and hence different radiative fluxes. For SS and DD the different underlying assumptions concerning particle size distributions lead to the differences seen in optical properties and radiative fluxes.

The differences between LW fluxes are smaller. The largest impact on the net LW radiation is due to DD, which is also the only species that appears different in the AOD experiments compared to the ZERO experiment (Figure 7d). In the MMR experiment series the SS and BC cases result in slightly smaller upward (negative) LW net fluxes on all model levels.

Preprints (www.preprints.org) | NOT PEER-REVIEWED | Posted: 17 January 2020 doi:10.20944/preprints202001.0183.v1

Table 6. Optical properties of aerosol species

EXPERIMENTS BASED ON AEROSOL CONCENTRATION AND OPTICAL PROPERTIES INPUT

Experiment	TAUSW$_s$ unitless	SSASW (0...1)	ASYSW (0...1)	TAULW$_s$ unitless	SSALW (0...1)	ASYLW (0...1)
MMR series						
MMR-SS	0.109	0.99	0.76	0.053	0.44	0.59
MMR-DD	0.310	0.97	0.68	0.092	0.34	0.36
MMR-OM	0.184	0.83	0.66	0.022	0.40	0.68
MMR-BC	0.363	0.15	0.27	0.015	0.00	0.00
MMR-SU	0.163	0.93	0.62	0.009	0.03	0.13

EXPERIMENTS BASED ON AOD550 INPUT

Experiment	TAUSW$_s$ unitless	SSASW (0...1)	ASYSW (0...1)	TAULW$_s$ unitless	SSALW (0...1)	ASYLW (0...1)
AOD series						
AOD-SS	0.213	0.99	0.77	0.006	0.60	0.39
AOD-DD	0.350	0.86	0.65	0.048	0.40	0.15
AOD-OM	0.293	0.89	0.63	0.002	0.27	0.15
AOD-BC	0.309	0.86	0.60	0.002	0.25	0.14
AOD-SU	0.293	0.89	0.63	0.002	0.27	0.15

As in Table 4 but for the MMR and AOD series of sensitivity experiments.

Finally, Table 6 shows the vertically integrated SW and LW optical properties for the sensitivity experiments. The maximum TAUSW$_s$ occurred when BC was used while the largest TAULW$_s$ was related to DD. TAULW$_s$ is 49% of TAUSW$_s$ in the MMR-SS experiment. For DD, TAULW$_s$ is 30% in MMR-DD but only 9% in the AOD-DD experiment. For all other species TAULW is an order of magnitude smaller than TAUSW in the MMR experiments, and two orders of magnitude smaller in the AOD experiments. The MMR-BC SSASW and SSASY show the smallest values (0.15 and 0.27) among all experiments This means that BC is highly absorbing and the small amount of scattering is diffusive. The other species are mostly (forward) scattering in the SW part of the spectrum. All species, with the exception of SS in AOD-SS, are more absorbing than scattering in the LW (SSALW < 0.5 in Table 6).

Figure 8 shows the vertical distributions of the optical properties of each category of aerosols in a similar way to Figures 4 and 5. The hydrophilic species - SS, OM and SU - show variations related to the vertical distribution of humidity while the hydrophobic DD and BC show smooth exponential distributions of TAUSW and TAULW and constant values in the vertical for SSA and ASY, in the SW and LW parts of the spectrum. The highly absorbing BC and highly scattering DD show the largest values of SWTAU. As discussed earlier (Section 3.4), both of these species played a role in the Badajoz experiments. In those experiments, the difference between the n.r.t and prescribed exponential vertical distributions explain the difference in SW transmission.

Note that in the sensitivity experiments, the total-column AOD550 or MMR values were assumed and distributed vertically using the default exponential profiles. The optical properties calculated in the MMR sensitivity experiments could be applied in future analyses of the differences between cases of different aerosol composition, like the Ladoga and Badajoz experiments here.

4. Discussion

In this study we suggest improvements to the aerosol radiative transfer parametrizations for use in the ALADIN-HIRLAM NWP system. The calculation of aerosol optical properties in the real-time

 doi:10.20944/preprints202001.0183.v1

atmospheric conditions was updated in HARMONIE-AROME, based on combination of the climatological 2D or n.r.t. 3D aerosol concentrations from CAMS and the new pre-calculated IOPs from ECMWF. The resulting AODs, SSAs, ASYs for the aerosol mixture at 30 LW and SW wavelengths were used to calculate broadband values of these optical parameters by applying spectral averaging over the SW (0.20-12.19 μm) and LW parts (3.08-1000 μm) of the spectrum.

These broadband optical properties were used by HLRADIA, the simplest radiation scheme available in HARMONIE-AROME, employing the approach in Enviro-HIRLAM [1,12]. The impact of the updated aerosol optical properties on the radiative fluxes and temperature tendencies was studied in single-column MUSC experiments. The atmospheric state and aerosol concentration, originating from CAMS, were extracted from 3D HARMONIE-AROME experiments. For additional sensitivity studies, artificial 2D AOD550 and MMR data were prepared and used as input.

Our main findings are summarised as follows:

When the aerosol load is at a background level, different methods of treating the aerosol concentration and optical properties lead only to small differences in the calculated radiation fluxes and radiative heating. When the concentration of some aerosol species is higher than its background level, regionally or during pollution episodes, reliable 3D aerosol data are more useful. To benefit from such data accurate treatment of the optical properties of the different species becomes important.

based on climatological AOD550 or MMR and those using n.r.t. data for the desert dust intrusion case over Badajoz. For example, SW transmission was 0.98 (0.97) when 2D climatological MMR (AOD550) was used but 0.78 when n.r.t. 3D MMR data or 2D AOD550 was used. For the same case, LW transmission was 0.90 when 3D or 2D MMR was used and 0.95 with 2D AOD550, but 0.98 and 1.0 in the 2D climatological MMR and AOD550-based experiments. In general, LW differences were smaller than SW differences. The minimum value of 0.78 for SW transmission seen in the Badajoz experiment is not very low. For example, based on satellite-based estimates [29] monthly mean values of less than 0.5 were recently reported over areas of India. Our example was that of desert dust. The aerosol composition over India is likely to be quite different.

Sensitivity studies, where an input of total-column AOD550=0.5 was assumed, demonstrated the impact of each aerosol species. To obtain such an AOD550 value, only 37 μg of black carbon, but almost one gram of sea salt, per square metre in the whole column was needed. SW transmission due to this amount of black carbon was 0.56 while it was 0.95 for the sea salt, both of which had the same AOD550 value. This demonstrates that it is important to account for the scattering and absorption properties of the different species, and not only to estimate the total AOD. When the same AOD550=0.5 input was handled using the old prescribed IOPs, the SW transmissivity increased to 0.79 for black carbon and decreased to 0.90 for sea salt. The smallest SW transmissivity value of 0.76 was for desert dust. On the other hand, these differences show that an uncertainty in the estimated concentration of the different species has different impacts: an error of one μg in the mass of black carbon might influence the radiative transfer more than a ten- or hundred-fold error in the estimation of the mass of coarser particles.

The difference between the AOD and MMR sensitivity experiments was in way they handle optical properties. Both relied on vertically integrated AOD or MMR values that were distributed vertically using the same exponential profiles, specific to each species. However, the optical properties depend on the vertical distribution of the aerosols and also on the atmospheric humidity that varies significantly with elevation. With the new way of combining the optical properties and aerosol mass distribution we introduced new sensitivities to the calculation of the radiative transfer, in particular concerning the vertical distribution of aerosol species.

Using the single-column model framework allowed us to diagnose effects and interactions that could not easily be detected from the results of 3D model experiments. The main limitations of our study include the following for which we suggest further experimenting and development:

Preprints (www.preprints.org) | NOT PEER-REVIEWED | Posted: 17 January 2020 doi:10.20944/preprints202001.0183.v1

- We have applied the simple HLRADIA scheme to determine the sensitivity of radiation fluxes and temperature tendencies to aerosol load and optical properties. HLRADIA was chosen for the practical reasons of availability and simplicity. Its known limitations, related to the simplified treatment of atmospheric layers and the use of many empirical coefficients for the calculation of the SW and LW radiative transfer, must be taken into consideration. In particular, HLRADIA is unable to fully benefit from the 3D details of the aerosol optical properties suggested here. Also, as a broadband scheme it is unable to treat the spectral details of aerosol-radiation interactions that may become important in the LW range of the spectrum.
- In our MUSC experiments the surface temperature was kept constant on purpose by assuming a water/ice surface at the bottom of the atmospheric column. Thus, only a minor change in the near-surface temperatures was detected due to the change in the surface radiation balance when the experiments were run beyond +24 hours (not shown). In reality, the local near-surface temperature changes that are related to aerosol impacts on radiation over land areas such as those shown earlier in the model-observation comparison for Badajoz [13], are assumed to arise from soil heating and not because of direct air temperature changes. However, MUSC is a less suitable tool for analysing the evolution of temperature and other atmospheric variables over time, due to the large-scale dynamical processes that are ignored in the single-column framework.
- We have analysed the impact of mineral dust in a Saharan dust intrusion case study. The impact of other aerosol species - sea salt, organic matter, black carbon and sulphates were only studied using artificial data under realistic atmospheric conditions. It would be interesting to study wildfire cases again, where organic matter, and possibly black carbon, impacts could be seen. Cases of increased volcanic and anthropogenic emissions deserve additional study. Stratospheric volcanic sulphates, that are assumed to be a main factor in past climate cooling episodes at annual to decadal scales (see [30] and references therein), were not included. Stratospheric aerosols are poorly parametrised in limited area NWP models and are not represented in the CAMS data used in this study. However, volcanic emissions contribute to the tropospheric sulphate and dust loads in the CAMS data.
- We did not carry out tests using 3D climatological MMR data, that is available from the CAMS reanalysis at relatively high horizontal and vertical resolution and used in the ECMWF model [6]. We believe that for a limited-area NWP model used for short-range weather forecasting, it is a higher priority to capture episodes of high aerosol load in real time than to address small systematic errors that may be related to the use of a coarse-resolution 2D aerosol climatology. The computing resources needed for the use of n.r.t. or climatological 3D data may be comparable.
- Cloud-radiation-aerosol interactions were excluded from this study in order to focus on the direct radiative effects of aerosols. It is possible to diagnose the first indirect effect of aerosols, namely the impact of (hydrophilic) aerosols on the evolution of cloud droplets towards precipitating particles. The effective size of cloud particles can be diagnosed and fed to the radiation schemes for a better estimation of the radiative transfer through clouds. Single-column experiments can be used as a first step for formulating and testing the parametrizations, to pave the way for 3D model experiments.

To overcome the limitations of single-column studies, 3D HARMONIE-AROME experiments are envisaged. They will allow the study of aerosol impacts on weather parameters, and will take dynamical processes and the evolving surface interactions of different surface conditions into account, as well as quantify aerosol-related uncertainties in weather forecasting. It is more reasonable to do such experiments using advanced radiation schemes that treat radiative exchange between atmospheric layers in cloudy and clear-sky cases. The results of 3D experiments should be compared to aerosol and radiation observations.

Preprints (www.preprints.org) | NOT PEER-REVIEWED | Posted: 17 January 2020 doi:10.20944/preprints202001.0183.v1

5. NWP Model and aerosol data

5.1. The Shared ALADIN-HIRLAM NWP System

The shared ALADIN-HIRLAM numerical weather prediction system [18], hereafter denoted the ALADIN-HIRLAM, is developed and maintained by those working in the ALADIN and HIRLAM NWP consortia. Many different configurations of the system are used by participating members, see Table 7 for abbreviations and references. The canonical configuration used by the authors of this paper is known as HARMONIE-AROME [23]. By default, HARMONIE-AROME includes two parametrizations of radiative transfer while a third scheme has been included in a development branch. Details on these radiation parametrizations are provided in Section 5.2. T

he single column configuration of the ALADIN-HIRLAM called MUSC (Modèle Unifié, Simple Colonne), was used for the sensitivity tests presented in this paper. This 1D tool has primarily been developed by Météo France [22] but has a growing user and developer base in both HIRLAM and ALADIN countries. The tool was initially developed for validating and comparing physical parametrizations in the NWP system. In an NWP system the dynamical and physical processes are split into vertical and horizontal contributions. For physical processes, the horizontal contributions are neglected making it possible to isolate a column from the full model. Nevertheless, MUSC shares the same source code as the 3D model and is therefore always kept up-to-date with recent developments.

MUSC requires an initial state of the atmosphere, surface and physiographic information as input. Forcings are needed to determine the tendencies due to advection from neighbouring columns. Both the initial state and atmospheric forcing can be extracted from the results of a full HARMONIE-AROME forecast for example. It is possible to provide a background state that the profile can relax towards during the time-integration. However, a profile can easily drift away from a realistic atmospheric state and there is no interaction with the large-scale flow which makes such a set-up unsuitable for real weather forecasting. MUSC is computationally very cheap and it is easy to replace parametrizations and to study problems by specifying forcings. This makes is a very useful tool for investigating model sensitivities. In this study we use MUSC in diagnostic, rather than forecasting, mode where we extract the output from the first time-step of the model integration to avoid the issues just mentioned. In diagnostic mode atmospheric forcings are not needed.

5.2. Radiation Schemes in HARMONIE-AROME

In this section we summarise the basic properties of three radiation schemes that are available within HARMONIE-AROME.

5.2.1. IFSRADIA

The scheme used by default is an old version of the European Centre for Medium-Range Weather Forecasts (ECMWF) radiation scheme from cycle 25R of their Integrated Forecasting System (IFS) [31, Section 2.2], in this paper denoted as IFSRADIA. This scheme has six shortwave and 16 longwave spectral bands. The optical properties of clouds are determined from temperature, cloud cover, cloud liquid, cloud ice content and cloud particle effective radii; the latter is parametrized. Ozone and aerosol (AOD550) climatologies are used, and with the exception of water vapour, which is a prognostic output variable, climatologies of other atmospheric gases are used. Overall, the scheme is computationally heavy and as a result is only called 4 to 5 times a hour during the forecast.

Preprints (www.preprints.org) | NOT PEER-REVIEWED | Posted: 17 January 2020 doi:10.20944/preprints202001.0183.v1

5.2.2. ACRANEB

The second scheme is a simpler, more computationally efficient, broadband scheme, called ACRANEB2 ([32,33], denoted ACRANEB in this paper). Versions of this scheme have been used in the ALADIN NWP model [18] since the 1990s. The optical properties of atmospheric gases, clouds, aerosols (AOD550) and the surface are derived from the data available within HARMONIE-AROME. ACRANEB includes an advanced treatment of LW interactions between the atmospheric layers resolved by the model. By default, cloud-radiation interactions are fully taken into accounted at each model time-step while the impact of atmospheric gases is calculated less frequently.

5.2.3. HLRADIA

The third scheme, included only in development versions of HARMONIE-AROME, is known as HLRADIA [25]. This scheme originates from the HIRLAM NWP model [34]. It is based on a pioneering study by Savijärvi [26], who suggested a quick and simple radiation scheme for mesoscale NWP models in which the SW and LW radiative transfer is parametrized by empirical fitting to detailed reference calculations. The radiative effects of atmospheric gases, ozone and aerosols are, by default, approximated using constant coefficients for the LW and SW intervals. This scheme is always called at every time step of the forecast run. Because this scheme was used for all of the sensitivity tests carried out in this study, further details about the parametrization are provided in the paragraph below.

SW and LW transmission and LW absorption are calculated for three atmospheric layers - a layer above the clouds, in the clouds themselves and below the clouds. Multiple cloud layers are treated as a single thick layer ignoring the clear-sky layers between them. For clear-sky cases the transmission/absorption is calculated for the entire atmospheric column. Diagnostic SW and LW net fluxes at each model level are calculated for the model output. The fluxes are obtained by integrating the parametrized temperature tendencies from the surface up to the TOA and using the net SW and LW fluxes at the surface as boundary conditions.

In the SW part of the spectrum HLRADIA estimates the clear-sky flux from the TOA either to the cloud top or to the surface, taking the overlying atmospheric conditions into account. Atmospheric heating due to SW absorption by gases, aerosols and cloud particles is calculated at each model level from the TOA down to the surface. However, the absorption of the scattered radiation is not explicitly taken into account. The HLRADIA parametrization of LW heating assumes that each atmospheric level cools to space and interacts with the surface and the layer of clouds, if there. This means that the interactions between adjacent model levels are ignored. LW heating is calculated at each model level using the average above/in/below-cloud transmission and absorption.

The outgoing radiative fluxes (LWUT and SWUT) at the TOA were found earlier to be mostly overestimated by HLRADIA compared to reference results when aerosols were excluded. Absorption of SW radiation by atmospheric gases appeared to be underestimated and LW absorption overestimated [25]. This is due to the simplified treatment of atmospheric layers in HLRADIA and the use of many empirical coefficients to calculate the SW and LW radiative transfer. These simplifications also influence the new aerosol radiative transfer parametrizations introduced to HLRADIA (Section 2).

5.3. CAMS Mass Mixing Ratios (MMR) and ECMWF IOP data

The 11 aerosol species [4,6] in the CAMS datasets describe the following 5 aerosol categories: sea salt (SS), mineral dust (DD), organic matter (OM), black carbon (BC) and sulphate (SU). Three size bins are used to describe the SS and DD aerosols. The bin limits for DD are 0.03, 0.55, 0.9 and 20 μm, while for SS they are 0.03, 0.5, 5 and 20 μm. For OM and BC hydrophilic and hydrophobic components are considered

 doi:10.20944/preprints202001.0183.v1

separately. In July 2019 CAMS was upgraded [35] to include three new aerosol fields representing nitrate and ammonium species. These new species have not been used in our experiments.

For this study, the monthly 2D CAMS MMR climatology [6,24] and 3D n.r.t. CAMS MMR data [5] were used. 11 aerosol species were used in each case. Input data (atmospheric and surface profiles) for the MUSC experiments were extracted from the output of corresponding 3D HARMONIE-AROME experiments as described below.

The global 2D MMR climatology and the corresponding IOPs of 11 aerosol species at 30 wavelengths were obtained from ECMWF courtesy of Alessio Bozzo (personal communication, December 2016). The monthly 2D MMR climatologies were introduced to a 3D HARMONIE-AROME experiment via the physiography (climate) generation step in the model. The 2.5-degree resolution data were interpolated bilinearly to the HARMONIE-AROME 2.5 km horizontal grid spacing. Once introduced to a HARMONIE-AROME experiment these aerosol data remain constant in time for the duration of the forecast.

3D n.r.t. CAMS aerosol data for needed dates were imported from CAMS +12h forecast output via 3D HARMONIE-AROME experiments. The horizontal resolution of the CAMS global forecasting system is T511, which means that the Gaussian grid is truncated at wavenumber N=256. At 45 degrees latitude the resolution is 0.35 degrees. In July 2019 the number of model levels in CAMS forecasts was increased to 137 [35], the same number as in ECMWF's high-resolution weather forecasting model. In this study, n.r.t. data with the previous vertical resolution of 60 levels was used. The n.r.t. CAMS MMR fields were interpolated to the HARMONIE-AROME grid of 2.5 km and 65 vertical levels and introduced via the background fields of the 3D variational data assimilation and lateral boundary conditions. The model dynamics advects the fields during the forecast run.

Calculation of the aerosol IOPs, prepared for the ECMWF models and used for HARMONIE-AROME in this study, is described in detail by Bozzo et al. [6]. A log-normal size distribution of spherical particles is assumed for all of the aerosol types in order to calculate the spectral ME, SSA and ASY for each aerosol type. For hydrophilic aerosol species hygroscopic growth is accounted for in the calculation of the optical properties. Organic matter represents a mixture of continental natural and anthrophogenic aerosols. The properties of black carbon and sea salt originate from OPAC [20]. Sulfate includes industrial, volcanic and biogenic emissions. The optical properties of dust follow [37]. Figure A1 in [6] presents the optical properties of various aerosol types.

The 3D broadband optical properties (AOD, SSA, ASY) of the aerosol mixture were derived for HLRADIA using ECMWF IOPs. The basic data for 11 species, 30 wavelengths and 10 relative humidities were converted to a lookup table, that is read at the initial step of each HARMONIE-AROME forecast. During each time-step of the forecast run, the relative humidity on the model's 3D grid is used to select the needed values of ME, SSA and ASY. The runtime AODs of 11 species at 30 wavelengths are calculated at each grid point by combining the wavelength-dependent ME to the location and height-dependent MMR fields. The optical properties of the aerosol mixture at each wavelength were calculated as a sum of AODs over the 11 species and the corresponding weighted averages of SSA and ASY. Finally, the weighted average over the 14 SW and 16 LW spectral bands defines the needed LW and SW broadband values of AOD, SSA and ASY of the aerosol mixture at each point of the 3D grid at each time step. For the spectral weighting, the wavelength distribution of solar and terrestrial radiation was applied as in [1].

6. Conclusions and outlook

Using external 3D aerosol concentration data instead of climatological AOD550 data is beneficial for limited-area NWP models for several reasons. Until now, the treatment of aerosol inputs has usually been a part of the radiation schemes. We suggest preparing the 3D optical properties (AOD, SSA, ASY) of

 doi:10.20944/preprints202001.0183.v1

the aerosol mixture at each time-step of the model's integration, taking the atmospheric humidity into account. Using the resulting actual optical properties as input will enable radiative transfer calculations to be done by any scheme without treating the specific properties of individual aerosol species. The possibility to choose between n.r.t. or climatological aerosol input data provides additional flexibility. Aerosol concentration data can also be used for cloud microphysics parametrizations. This also opens the way for improved consistency between radiation and cloud parametrizations, in particular regarding the derivation and use of cloud particle effective sizes.

In this study we have taken the external aerosol data and IOPS as given, and focused on ways to use these in a limited-area NWP model. Global integrated weather-chemistry models, with advanced data assimilation, produce presumably more reliable data than any regional model would do. The CAMS global reanalysis data [4] are more detailed and more reliable than the old Tegen dataset [19]. However, the results from global weather-chemistry models contain uncertainties related to aerosol emission sources, assumptions used in the data assimilation, parametrizations of aerosol dynamics and the derivation of IOPs that have been discussed extensively in recent papers [4,6] documenting the CAMS reanalysis. Additional inaccuracies arise from the spatial and temporal interpolation of the coarse-resolution global aerosol data to the high-resolution limited-area NWP model grid.

Based on our results, we suggest the following steps for improving aerosol-related parametrizations in the ALADIN-HIRLAM NWP system:

- Introduce MMR-based 3D optical properties of the aerosol mixture to the IFSRADIA and ACRANEB radiation schemes in order to benefit from the more advanced SW and LW radiation transfer parametrizations in these schemes compared to HLRADIA
- Implement the method of importing n.r.t. high-resolution 3D CAMS MMR data to the ALADIN-HIRLAM system for operational use. Investigate possible simplifications to save computational resources.
- Carry out extensive model-observation inter-comparisons for biomass burning, mineral dust intrusion, anthrophogenic and volcanic emission case studies in order to evaluate their impacts on local weather and radiation flux forecasts.
- Find optimal ways to use n.r.t. aerosol concentration data in cloud-precipitation microphysics parametrizations. Utilizing such data, evaluate cloud particle effective size, which is assumed to be the key parameter in the consistent treatment of aerosol-cloud-radiation interactions.

Author Contributions: :

LR introduced the renewed aerosol optical properties and climatological aerosol concentrations to the ALADIN-HIRLAM NWP system, designed and ran the MUSC experiments and prepared the original manuscript draft; EG participated in preparation and running of the MUSC experiments and edited the final text; DM introduced the n.r.t. CAMS aerosol to the ALADIN-HIRLAM system; KPN is the author of the aerosol transfer code for HLRADIA, originally for Enviro-HIRLAM; VT was the first to introduce external climatological aerosol data and IOPs to the ALADIN-HIRLAM system. All authors contributed to the analysis of results, and writing and editing the manuscript.

Funding: This research received no external funding.

Acknowledgments: We would like to thank Alessio Bozzo for the CAMS global aerosol MMR climatology and ECMWF aerosol optical properties datasets. Support of the international HIRLAM-C programme is also acknowledged.

Conflicts of Interest: The authors declare no conflict of interest.

Abbreviations

 doi:10.20944/preprints202001.0183.v1

Table 7. Glossary of the ALADIN-HIRLAM system

Acronym	Full name	Purpose	Note
ALADIN-HIRLAM		Limited area nonhydrostatic NWP system	Termonia et al. [18]
ALADIN	Aire Limitée Adaptation Dynamique Développement International	Limited area NWP model and consortium	Since 1990
HIRLAM	High Resolution Limited Area Model	Limited area NWP model and consortium	Since 1985
AROME	Application of Research to Operations at Mesoscale	NWP configuration of ALADIN	Seity et al. [36]
HARMONIE	HIRLAM ALADIN Research for Mesoscale NWP in Europe	Configuration within ALADIN-HIRLAM	Since 2007
HARMONIE-AROME		AROME configuration within HARMONIE	Bengtsson et al. [23]
MUSC	Modèle Unifié, Simple Colonne	Single column version of the system	Malardel et al. [22]

References

1. Baklanov, A., D. Brunner, G. Carmichael, J. Flemming, S. Freitas, M. Gauss, Ø. Hov, R. Mathur, K.H. Schlünzen, C. Seigneur, and B. Vogel, 2017: Key Issues for Seamless Integrated Chemistry–Meteorology Modeling. Bull. Amer. Meteor. Soc., 98, 2285–2292, https://doi.org/10.1175/BAMS-D-15-00166.1, 2017a.
2. Baklanov, A., Smith Korsholm, U., Nuterman, R., Mahura, A., Nielsen, K. P., Sass, B. H., Rasmussen, A., Zakey, A., Kaas, E., Kurganskiy, A., Sørensen, B., and González-Aparicio, I.: Enviro-HIRLAM online integrated meteorology–chemistry modelling system: strategy, methodology, developments and applications (v7.2), G *Geosci. Model Dev.*, 10, 2971–2999, https://doi.org/10.5194/gmd-10-2971-2017, 2017b.
3. Flemming, J., Peuch, V.-H., and Jones, L.: Ten years of forecasting atmospheric composition at ECMWF, ECMWF newsletter 152, available at: https://www.ecmwf.int/en/newsletter/152/news/ten-years-forecasting-atmospheric-composition-ecmwf (last access: 1 January 2020), 2017.
4. Inness, A., Ades, M., Agustí-Panareda, A., Barré, J., Benedictow, A., Blechschmidt, A.-M., Dominguez, J. J., Engelen, R., Eskes, H., Flemming, J., Huijnen, V., Jones, L., Kipling, Z., Massart, S., Parrington, M., Peuch, V.-H., Razinger, M., Remy, S., Schulz, M., and Suttie, M.: The CAMS reanalysis of atmospheric composition, Atmos. Chem. Phys., 19, 3515–3556, https://doi.org/10.5194/acp-19-3515-2019, 2019.
5. Copernicus Atmosphere Monitoring Service (CAMS). https://atmosphere.copernicus.eu/data, 2019. Last access January 1, 2020.
6. Bozzo, A., Benedetti, A., Flemming, J., Kipling, Z., and Rémy, S.: An aerosol climatology for global models based on the tropospheric aerosol scheme in the Integrated Forecasting System of ECMWF, Geosci. Model Dev. Discuss., https://doi.org/10.5194/gmd-2019-149, in review, 2019.
7. Freitas, S.: Evaluating aerosols impacts on numerical weathe prediction: a WGNE/WMO initiative, available as: https://presentations.copernicus.org/EGU2015-7360_presentation.pdf. 2015, last access 12 January 2020.
8. Poliukhov, A.A., Chubarova, N.E., Blinov, D.V. et al. *Russ. Meteorol. Hydrol.*,44, 579-587, https://doi.org/10.3103/S1068373919090012, 2019.
9. Mulcahy, J. P., Walters, D. N., Bellouin, N., and Milton, S. F.: Impacts of increasing the aerosol complexity in the Met Office global numerical weather prediction model, *Atmos. Chem. Phys.*, 14, 4749-4778, https://doi.org/10.5194/acp-14-4749-2014, 2014.
10. Rémy, S., Kipling, Z., Flemming, J., Boucher, O., Nabat, P., Michou, M., Bozzo, A., Ades, M., Huijnen, V., Benedetti, A., Engelen, R., Peuch, V.-H., and Morcrette, J.-J.: Description and evaluation of the tropospheric aerosol scheme

in the European Centre for Medium-Range Weather Forecasts (ECMWF) Integrated Forecasting System (IFS-AER, cycle 45R1), Geosci. Model Dev., 12, 4627–4659, https://doi.org/10.5194/gmd-12-4627-2019, 2019.

11. Fiedler, S., Kinne, S., Huang, W. T. K., Räisänen, P., O'Donnell, D., Bellouin, N., Stier, P., Merikanto, J., van Noije, T., Makkonen, R., and Lohmann, U.: Anthropogenic aerosol forcing – insights from multiple estimates from aerosol-climate models with reduced complexity, *Atmos. Chem. Phys.*, 19, 6821–6841, https://doi.org/10.5194/acp-19-6821-2019, 2019.
12. Gleeson, E., Toll, V., Nielsen, K. P., Rontu, L., and Mašek, J.: Effects of aerosols on clear-sky solar radiation in the ALADIN-HIRLAM NWP system, *Atmos. Chem. Phys.*, **16**, 5933-5948, https://doi.org/10.5194/acp-16-5933-2016, 2016.
13. Rontu, L., Pietikäinen, J.-P., and Martin Perez, D.: Renewal of aerosol data for ALADIN-HIRLAM radiation parametrizations, Adv. Sci. Res., 16, 129–136, https://doi.org/10.5194/asr-16-129-2019, 2019.
14. Toll V., Gleeson E., Nielsen K. P., Mannik, A., Mašek, J., Rontu, L. and Post, P.: Impacts of the direct radiative effect of aerosols in numerical weather prediction over Europe using the ALADIN-HIRLAM NWP system. *Atmospheric Research*, 163–173. https://doi.org/10.1016/j.atmosres.2016.01.003, 2016.
15. N. Bellouin, J. Quaas, E. Gryspeerdt, S. Kinne, P. Stier, D. Watson-Parris, O. Boucher, K.S. Carslaw, M. Christensen 5 , A.-L. Daniau, J.-L. Dufresne, G. Feingold, S. Fiedler 4 , P. Forster, A. Gettelman, J. M. Haywood, U. Lohmann, F. Malavelle, T. Mauritsen, D.T. McCoy, G. Myhre, J. Mülmenstädt, D. Neubauer, A. Possner, M. Rugenstein, Y. Sato, M. Schulz, S. E. Schwartz, O. Sourdeval, T. Storelvmo, V. Toll, D. Winker, and B. Stevens: Bounding global aerosol radiative forcing of climate change. *Rev. Geoph.*, 00, 000–001, 2019. https://doi.org/10.1029/2019RG000660.
16. Toll, V., Christensen, M., Quaas, J., Bellouin, N.. Weak average liquid-cloud-water response to anthropogenic aerosols. *N*ature **2019**, *5*72, 51–55, 10.1038/s41586-019-1423-9.
17. Baklanov, A., Schlünzen, K., Suppan, P., Baldasano, J., Brunner, D., Aksoyoglu, S., Carmichael, G., Douros, J., Flemming, J., Forkel, R., Galmarini, S., Gauss, M., Grell, G., Hirtl, M., Joffre, S., Jorba, O., Kaas, E., Kaasik, M., Kallos, G., Kong, X., Korsholm, U., Kurganskiy, A., Kushta, J., Lohmann, U., Mahura, A., Manders-Groot, A., Maurizi, A., Moussiopoulos, N., Rao, S. T., Savage, N., Seigneur, C., Sokhi, R. S., Solazzo, E., Solomos, S., Sørensen, B., Tsegas, G., Vignati, E., Vogel, B., and Zhang, Y.: Online coupled regional meteorology chemistry models in Europe: current status and prospects, *Atmos. Chem. Phys.*, 14, 317–398, https://doi.org/10.5194/acp-14-317-2014,2014, 2014.
18. Termonia, P., Fischer, C., Bazile, E., Bouyssel, F., Brožková, R., Bénard, P., Bochenek, B., Degrauwe, D., Derkova, M., El Khatib, R., Hamdi, R., Mašek, J., Pottier, P., Pristov, N., Seity, Y., Smolíková, P., Spaniel, O., Tudor, M., Wang, Y., Wittmann, C., and Joly, A.: The ALADIN System and its canonical model configurations AROME CY41T1 and ALARO CY40T1, *Geosci. Model Dev.*, **11**, 257-281, https://doi.org/10.5194/gmd-11-257-2018, 2017.
19. Tegen, I., Hoorig, P., Chin, M., Fung, I., Jacob, D. and Penner, J.: Contribution of different aerosol species to the global aerosol extinction optical thickness: Estimates from model results. *J. Geophys. Res.*, **102**, 23895–23915, https://doi.org/10.1029/97JD01864, 1997.
20. Hess, M., Koepke, P., and Schult, I.: Optical Properties of Aerosols and Clouds: The Software Package OPAC. Bull. of the Amer. Met. Soc., 79, 5, 831-844, 1998.
21. Koepke, P., Hess, M., Schult, I., and Shettle, E. P.: Global Aerosol Data Set, Report No. 243, Max-Planck-Institut für Meteorologie, Hamburg, Germany, ISSN 0937-1060, 1997.

22. Malardel, S., de Bruijn, C., and de Rooy, W. A Single Column Model of HARMONIE in KNMI Parametrization Testbed (CY33T1 version) (KNMI Report), De Bilt, the Netherlands, available at: http://netfam.fmi.fi/muscwd11/docCY33.knmi.pdf (last access: 6 December 2019), 2010.
23. Bengtsson, L., Andrae, U., Aspelien, T., Batrak, Y., Calvo, J., de Rooy, W., Gleeson, E., Hansen-Sass, B., Homleid, M., Hortal, M., Ivarsson, K., Lenderink, G., Niemelä, S., Pagh Nielsen, K., Onvlee, J., Rontu, L., Samuelsson, P., Santos Muñoz, D., Subias, A., Tijm, S., Toll, V., Yang, X. and Ødegaard Køltzow, M.: The HARMONIE-AROME model configuration in the ALADIN-HIRLAM NWP system, Mon. Weather Rev., 145, 1919–1935, https://doi.org/10.1175/MWR-D-16-0417.1, 2017.
24. Bozzo, A, Remy, S, Benedetti, A, Flemming, J, Bechtold, P, Rodwell, MJ, Morcrette, J-J.: Implementation of a CAMS-based aerosol climatology in the IFS, *Technical Memorandum*,801. Available at www.ecmwf.int/en/elibrary/17219-implementation-cams-based-aerosol-climatology-ifs, last cited 1.1.2020.
25. Rontu L., Gleeson, E., Räisänen, P., Nielsen, K. P., Savijärvi, H. and Sass, B. H.: The HIRLAM fast radiation scheme for mesoscale numerical weather prediction models. *Adv. Sci. Res*, **14**, 195–215,https://doi.org/10.5194/asr-14-195-2017, 2017.
26. Savijärvi, H.: Fast Radiation Parameterization Schemes for Mesoscale and Short-Range Forecast Models, *J. Appl. Meteorol.*, **29**, 437–447, 1990.
27. Tanré, D., Geleyn, J. F., and Slingo, J.: First results of the introduction of an advanced aerosol-radiation interaction in the ECMWF low resolution global model, in: Aerosols and their climatic effects, edited by: Gerber, H. E. and Deepak, A., A. Deepak Publishing, Hampton, Va, USA, 133–177, 1984.
28. Joseph, J.H., W.J. Wiscombe, and J.A. Weinman, 1976: The Delta-Eddington Approximation for Radiative Flux Transfer. J. Atmos. Sci., 33, 2452–2459, https://doi.org/10.1175/1520-0469(1976)033<2452:TDEAFR>2.0.CO;2, 1976.
29. Lukose, L. and Dutta, D.: Estimation of aerosol corrected surface solar irradiance at local incidence angle over different physiographic sub-divisions of India and adjoining areas using MODIS and SRTM data. *J. Atmos. Oceanic Technol.*, https://doi.org/10.1175/JTECH-D-18-0202.1, 2019.
30. Rinne, J. and Alestalo, M.:. Volcanic impacts dominate bidecadal-multidecadal temperature variations during the late Holocene in Northern Fennoscandia. Journal of Geophysical Research: Atmospheres, 124, 11661– 11671. https://doi.org/10.1029/2019JD030864, 2019.
31. ECMWF. IFS documentation, Chapter 2, 2015. Available at: http://www.ecmwf.int/sites/default/files/elibrary/2015/9211-part-iv-physical-processes.pdf. Last access January 1, 2020.
32. Geleyn J. F., Mašek, J., Brožková, R., Kuma, P., Degrauwe, D., Hello G. and Pristov, N.: Single interval longwave radiation scheme based on the net exchanged rate decomposition with bracketing. *Q. J. R. Meteor. Soc.*, https://doi.org/10.1002/qj.3006, 2017.
33. Mašek, J., Geleyn, J. F., Brožková, R., Giot, O., Achom H. O. and Kuma, P.: Single interval shortwave radiation scheme with parameterized optical saturation and spectral overlaps. *Q. J. Roy. Meteor. Soc.*, **142**, pp. 304-326, https://doi.org/10.1002/qj.2653, 2016.
34. Undén, P., Rontu, L., Arvinen, H., Lynch, P., Calvo, J., Cats, G., Cuxart, J., Eerola, K., Fortelius, C., Garcia-Moya, J.A., Jones, C., Lenderlink, G., McDonald, A., McGrath, R., Navascues, B., Woetman Nielsen, N., Odegaard, V., Rodriguez, E., Rummukainen, M., Room, R., Sattler, K., Hansen Sass, B., Savijärvi, H., Wichers Schreur, B.,

 doi:10.20944/preprints202001.0183.v1

Sigg, R., The, H., Tijm, A., 2002. The HIRLAM version 5.0 model. HIRLAM documentation manual (HIRLAM Scientific Documentation). Available at hirlam.org.

35. ECMWF news release. Upgrade improves global air quality forecasts. https://www.ecmwf.int/en/about/media-centre/news/2019/upgrade-improves-global-air-quality-forecasts, 2019. Last access January 1, 2020.
36. Seity, Y., P. Brousseu, S. Malardel, G. Hello, P. Benard, F. Bouttier, C. Lac, and V. Masson, 2011: The AROME-France convective-scale operational model. *Mon. Wea. Rev.*, **139**, 976–991, https://doi.org/10.1175/2010MWR3425.1
37. Woodward, S.: Modeling the atmospheric life cycle and radiative impact of mineral dust in the Hadley Centre climate model, J. Geophys. Res., 106(D16), 18155-18166, 10.1029/2000JD900795, 2001.

Preprints (www.preprints.org) | NOT PEER-REVIEWED | Posted: 17 January 2020 doi:10.20944/preprints202001.0183.v1

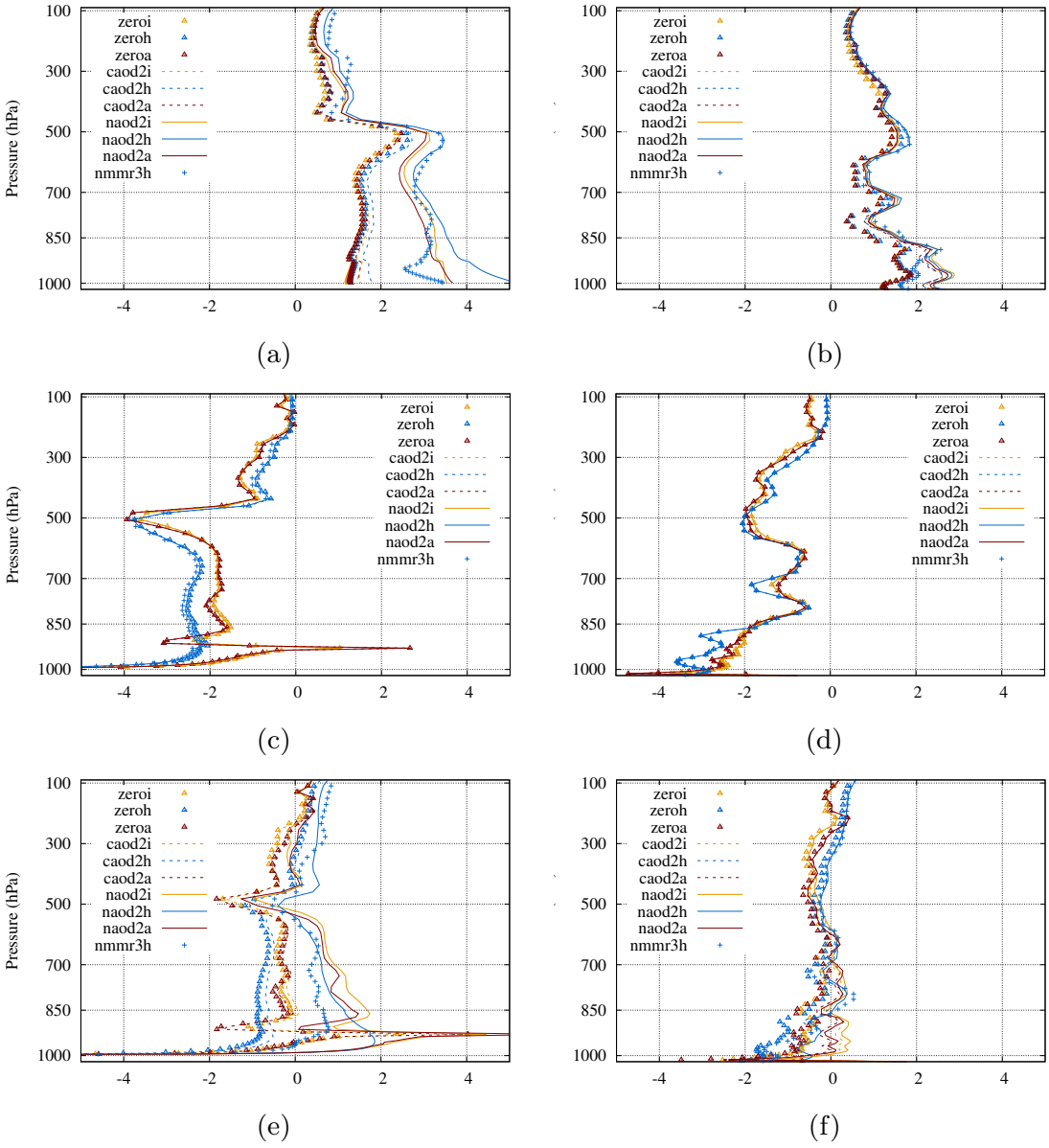

Figure 1. Temperature tendencies due to radiation (K/day) for Badajoz (left column) and Ladoga (right column): SW tendency (a, b), LW tendency (c, d), total tendency (e, f). y-axis shows pressure in hPa. Coloured curves correspond to the experiments and are labelled in the legends according to Table 1. The last letter in the label name denotes the radiation scheme with i for IFSRADIA, h for HLRADIA and a for ACRANEB.

Preprints (www.preprints.org) | NOT PEER-REVIEWED | Posted: 17 January 2020 doi:10.20944/preprints202001.0183.v1

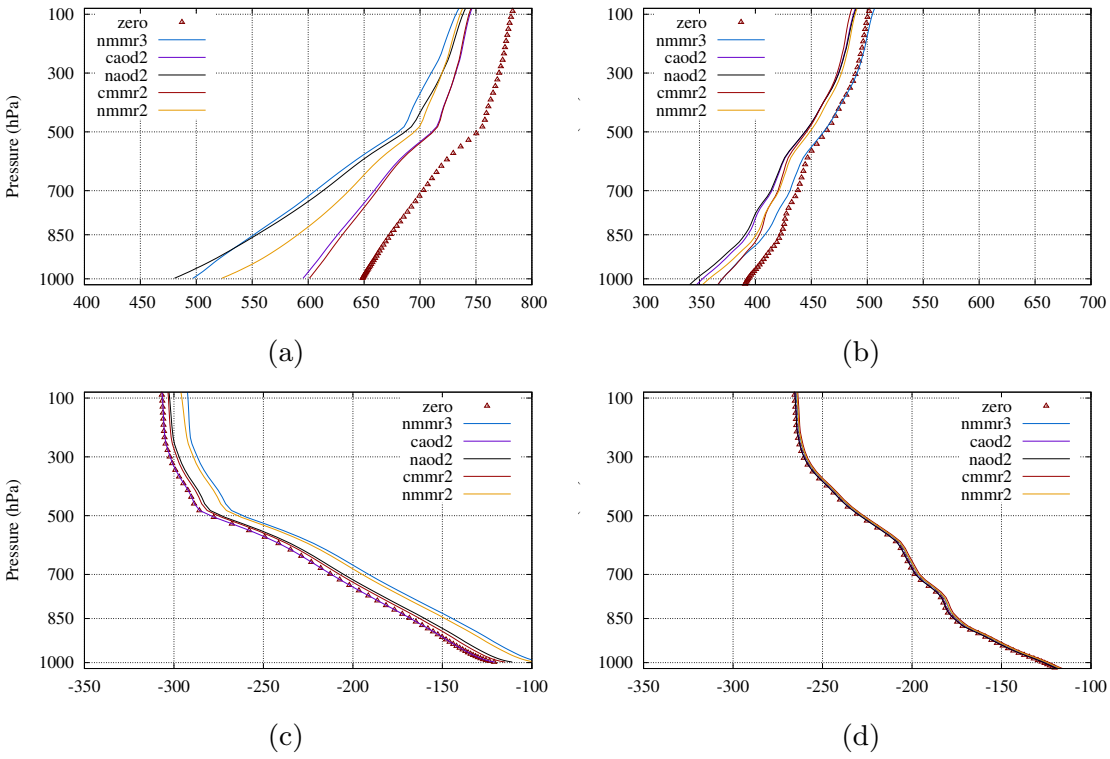

Figure 2. Net HLRADIA radiative fluxes (Wm^{-2}) for Badajoz (left) and Ladoga (right): SW (a, b) and LW (c, d). The curves correspond to the experiments in Table 1.

Preprints (www.preprints.org) | NOT PEER-REVIEWED | Posted: 17 January 2020 doi:10.20944/preprints202001.0183.v1

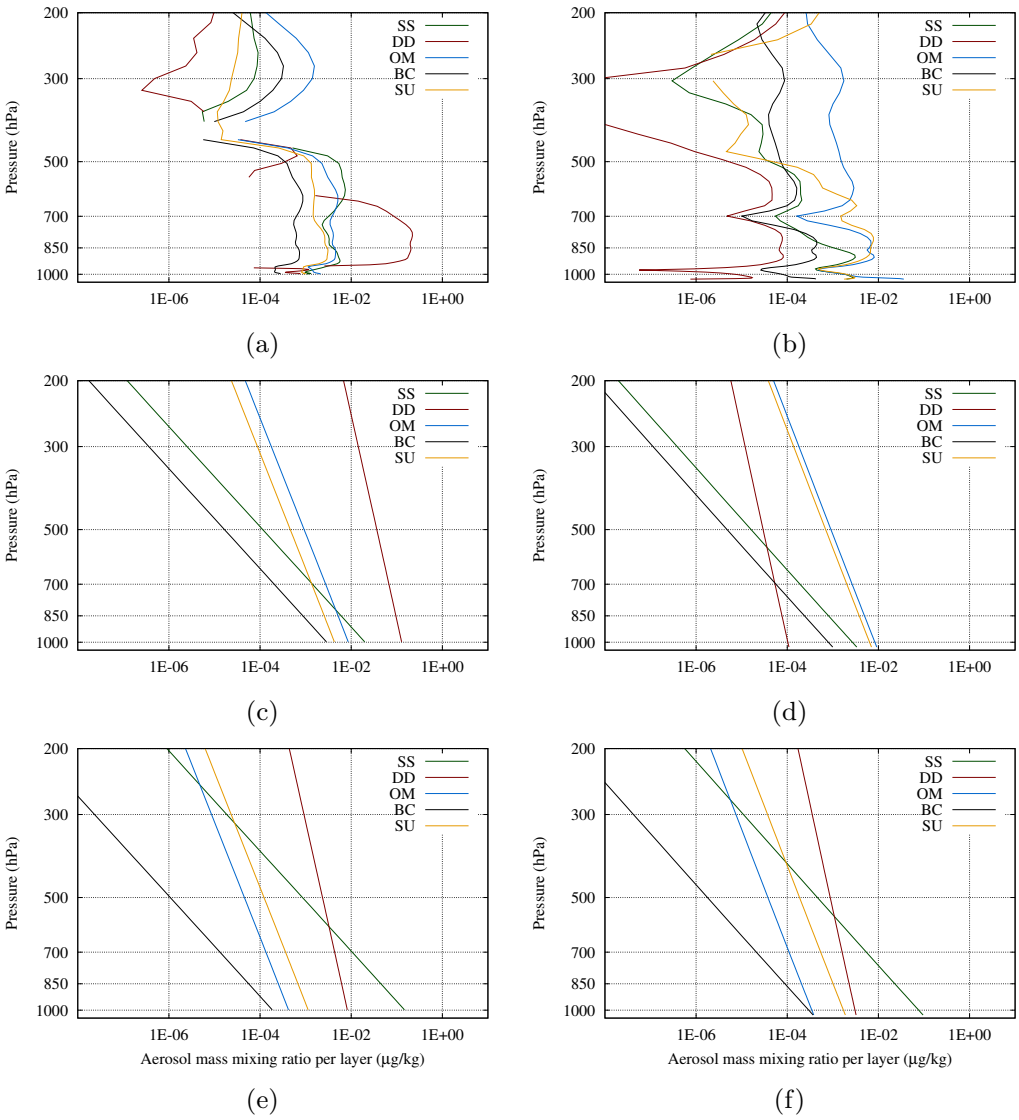

Figure 3. MMR (μg/kg) profiles for the (a, b) NMMR3 experiments, (c, d) NMMR2 and (e, f) CMMR2 over Badajoz (left)and Ladoga (right). y-axis shows pressure in hPa. Note the logarithmic scale on both axes.

Preprints (www.preprints.org) | NOT PEER-REVIEWED | Posted: 17 January 2020 doi:10.20944/preprints202001.0183.v1

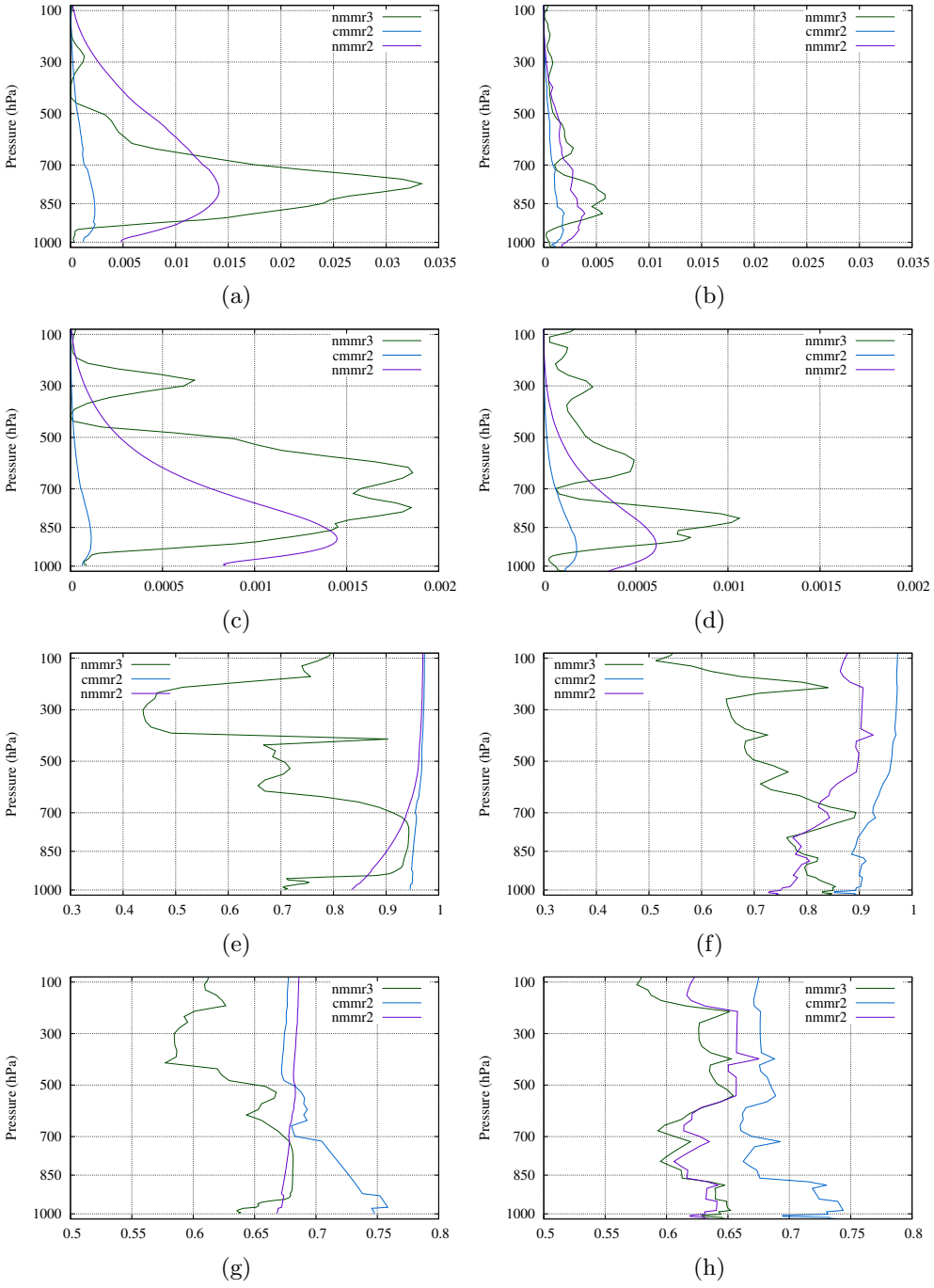

Figure 4. Profiles of the aerosol SW optical properties for Badajoz (left) and Ladoga (right): TAUSW (a,b), SWTAUA (c,d), SSASW (e,f), ASYSW (g,h). The acronyms are explained in Table 4. Names in the curve legends correspond to the experiments in Table 1.

Preprints (www.preprints.org) | NOT PEER-REVIEWED | Posted: 17 January 2020 doi:10.20944/preprints202001.0183.v1

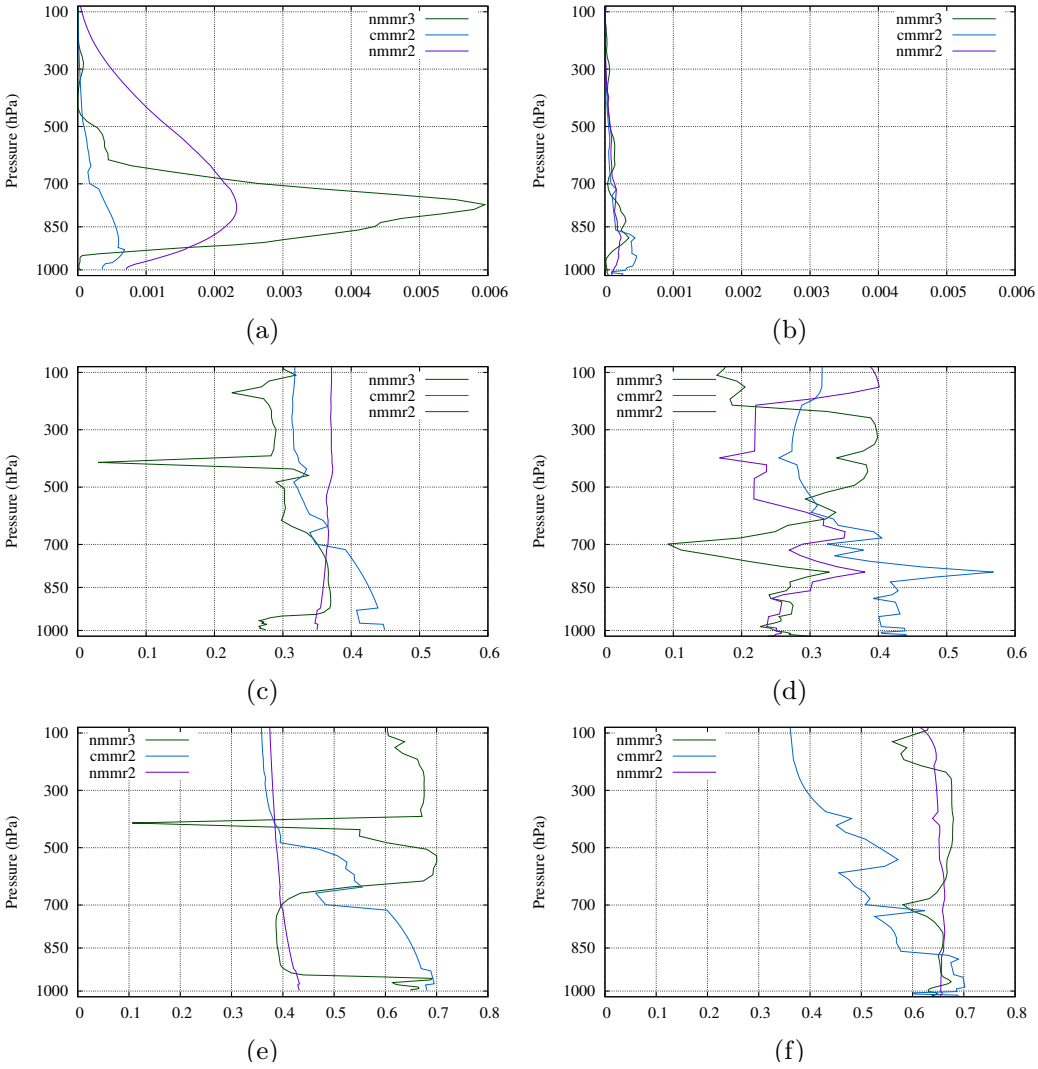

Figure 5. As in Figure 4 but for aerosol LW optical properties.

Preprints (www.preprints.org) | NOT PEER-REVIEWED | Posted: 17 January 2020 doi:10.20944/preprints202001.0183.v1

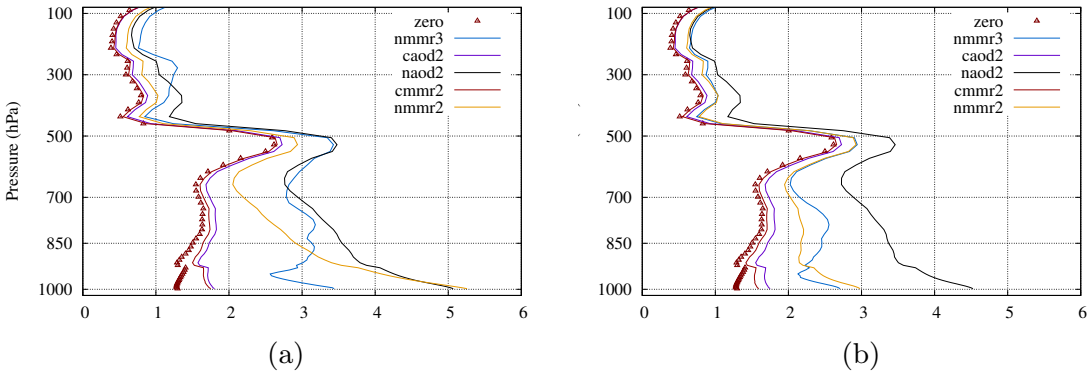

Figure 6. Temperature tendencies due to SW radiation (K/day) for Badajoz: (a) all species included (b) black carbon excluded. y-axis shows pressure in hPa. Figure legends correspond to the experiments as given in Table 1.

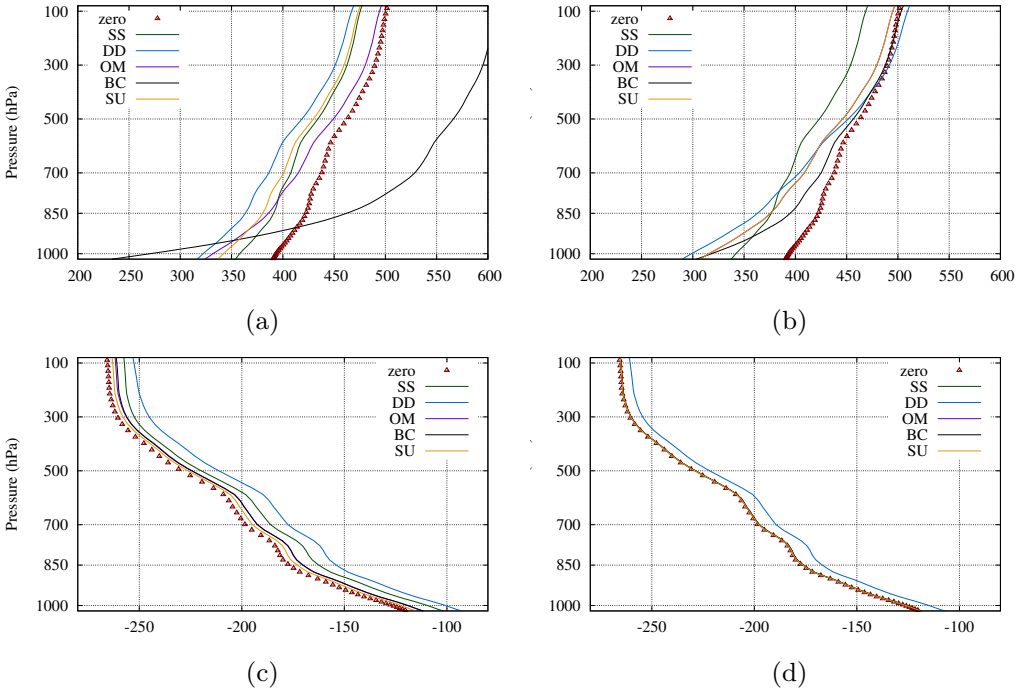

Figure 7. Net radiative fluxes (Wm^{-2}) for the MMR (left) and AOD550 (right) series of experiments: (a,b) SW and (c,d) LW. Figure legends correspond to the experiments as given in Table 1. SWD TOA = 779 Wm^{-2} (conditions over Lake Ladoga).

Preprints (www.preprints.org) | NOT PEER-REVIEWED | Posted: 17 January 2020 doi:10.20944/preprints202001.0183.v1

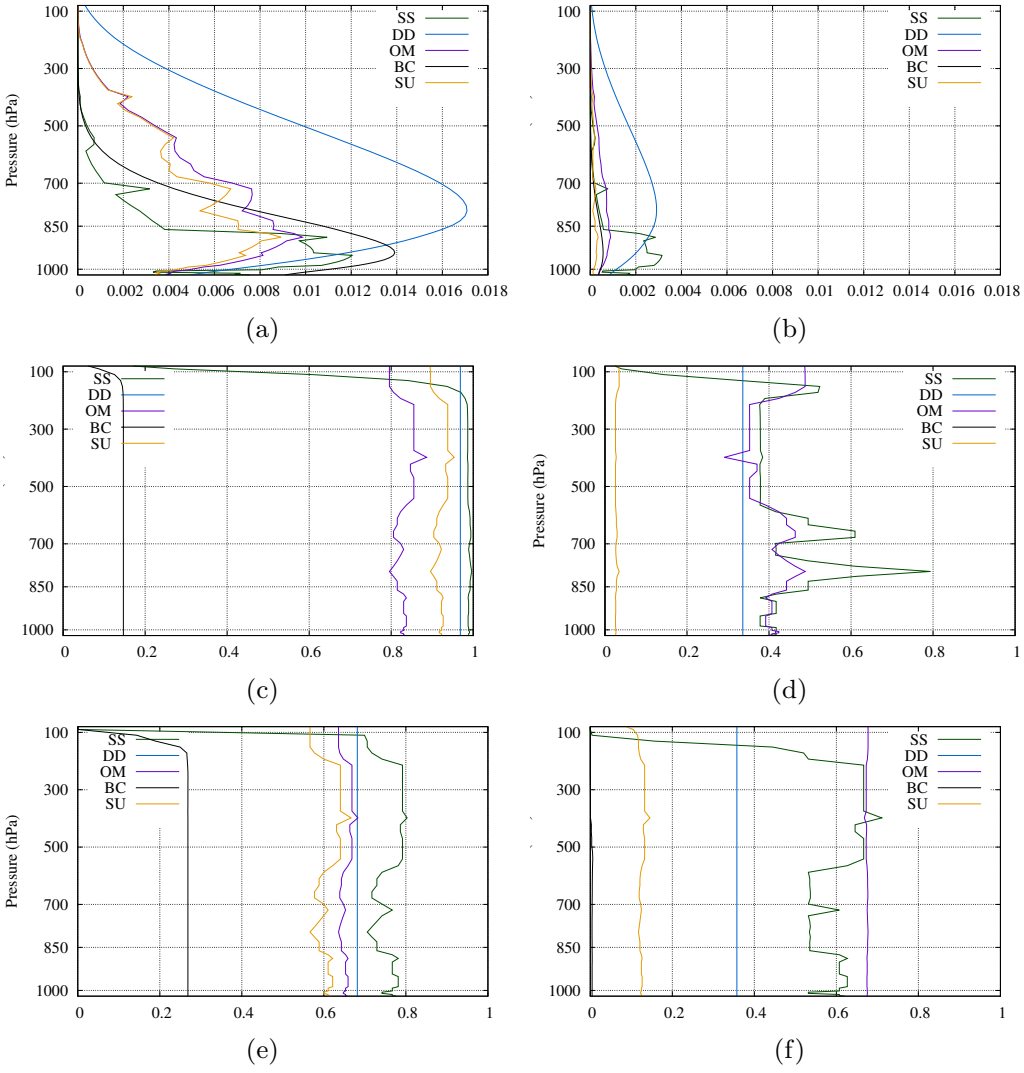

Figure 8. Profiles of aerosol SW (left) and LW (right) optical properties for the five aerosol species in the MMR series of experiments: (a) TAUSW, (b) TAULW, (c) SSASW, (d) SSALW, (e) ASYSW and (f) ASYLW. Acronyms are explained in Tables 3 and 4. The figure legends correspond to the experiments according to Table 1.